RESEARCH ARTICLE

A Novel Control Methodology Based on the Combination of TIDF and PID$^\mu$D Controllers Enhanced by the Orca Predation Algorithm for a Hybrid Microgrid System Involving Electric Vehicles

MOHAMMED H. ALQAHTANI[1], **(Member, IEEE), ALI S. ALJUMAH**[1],
SULAIMAN Z. ALMUTAIRI[1], **SEADA HUSSEN ADEM**[2], **ADEL OUBELAID**[3],
AND KAREEM M. ABORAS[4]

[1]Electrical Engineering Department, College of Engineering, Prince Sattam Bin Abdulaziz University, Alkharj 11942, Saudi Arabia
[2]School of Electrical and Computer Engineering, Haramaya Institute of Technology, Diredawa 202001, Ethiopia
[3]Laboratoire de Technologie Industrielle et de l'Information, Faculté de Technologie, Université de Bejaia, Bejaia 06000, Algeria
[4]Department of Electrical Power and Machines, Faculty of Engineering, Alexandria University, Alexandria 21544, Egypt

Corresponding authors: Mohammed H. Alqahtani (mh.alqahtani@psau.edu.sa), Seada Hussen Adem (seada.hussen@aastu.edu.et), and Kareem M. Aboras (kareem.aboras@alexu.edu.eg)

ABSTRACT In this study, an innovative mixed regulator based on integer and fractional order control is suggested for load frequency management. Tilt Integral Derivative with Filter (TIDF) and Proportional Integral Derivative Fractional Derivative with Filter (PID$^\mu$D) are the two components of the suggested hybrid, which is called TIDF-PID$^\mu$D. The advantages of the TIDF, the PIDD, and the fractional derivative regulators are combined in the proposed TIDF-PID$^\mu$D regulator. In order to enhance the suggested TIDF-PID$^\mu$D parameters in the investigated dual-area power grids, an innovative technique is used that is based on the newly reported Orca Predation Algorithm (OPA). The suggested TIDF-PID$^\mu$D regulator is part of a centralized control plan that takes into account the role of electric vehicles (EVs). Comparing the performance of the proposed TIDF-PID$^\mu$D regulator against that of previously published FOI-TD and PIDD2-PD associated with filters provides promising outcomes. In addition, the OPA optimizer's outcomes are contrasted to those of newly published optimization techniques such as the Gorilla Troops Optimizer (GTO), Gradient Based Optimizer (GBO), Battle Royale Optimizer (BRO), and Remora Optimization Algorithm (ROA), and the OPA optimizer has been shown to achieve better results. Taking into account non-linear limitations and the existence of renewable energy sources (RES) such as solar farms, wind farms, and EVs, this study examines the issue of frequency stability in a hybrid dual-area power system with thermal and hydraulic turbines. In ending, a sensitivity analysis has been carried out to prove the robustness and reliability of the proposed control structure. The results of this study are presented in the form of time-domain simulations that have been done with the assistance of MATLAB/SIMULINK (R2022a).

INDEX TERMS Orca predation algorithm (OPA), frequency stability, electric vehicle modeling, fractional order control, hybrid two-are power system, renewable sources, PIDD controller.

NOMENCLATURE

TIDF	Tilt Integral Derivative with Filter.
PID$^\mu$D	Proportional Integral Derivative Fractional Derivative with Filter.

The associate editor coordinating the review of this manuscript and approving it for publication was Shiwei Xia.

OPA	Orca Predation Algorithm.
GTO	Gorilla Troops Optimizer.
BRO	Battle Royale Optimizer.
ROA	Remora Optimization Algorithm.
EVs	Electric Vehicles.
RES	Renewable Energy| Sources.
GBO	Gradient Based Optimizer.
V2G	Vehicle-to-Grid.
LFC	Load Frequency Control.
CTDs	Communication Time Delays.
GRC	Generation Rate Constraint.
GDB	Governor Dead Band.
SOC	State of Charge.
ΔF_x	Frequency Fluctuation in Area x.
ΔF_y	Frequency Fluctuation in Area y.
ΔP_{tie}	Tie-line Power Fluctuation.
Kd_b	Derivative Action of The PID $^{\mu}$D Controller.
Ka_b	Acceleration Action of The PID $^{\mu}$D Controller.
μ	Derivative FO Operator of The PID $^{\mu}$D Controller.
STC	Standard Test Conditions.
PV	Photovoltaic.
FF	Fitness Function.
ITSE	Integral Timed Squared Error.
FO	Fractional Order.
Max.OS	Maximum Overshoot.
Max.US	Maximum Undershoot.
ST	Settling Time.
Kt_a	Tilt Action of The TIDF Controller.
Ki_a	Integral Action of The TIDF Controller.
Kd_a	Derivative Action of The TIDF Controller.
n	Tilt FO power.
Kp_b	Proportional Action of The PID $^{\mu}$D Controller.
Ki_b	Integral Action of The PID $^{\mu}$D Controller.
N_1, N_2, N_3	Noise Filtering Parameters.

I. INTRODUCTION

A. BACKGROUND

The availability of reliable and affordable electrical power has been important to the advancement of technology for decades. Because of rising levels of both population and technology, there has been a significant uptick in the rate at which power is consumed. In the past, conventional, non-renewable sources of energy powered installations in the energy sector. Concerns, on the other hand, are turning away from these sources because of their scarcity, the unfavorable consequences that they have on the environment, and the integration of renewable energy sources, abbreviated as RESs [1]. It is vital to place a greater emphasis on sustainable development to substitute traditional resources with renewable energy sources (RESs) such as wind and solar energy, biomass, geothermal, and so on.

Furthermore, the manipulation of energy storage units to enhance power networks that are based on green energy has gained substantial interest from researchers, corporations, and government incentives and regulations. Moreover, the collaborative management of electric automobiles that have been installed has also garnered major interest. They have the potential to contribute to preserving the robustness and dependability of power systems [2]. In addition, by implementing contemporary single- and multiple-constraint optimization approaches, such as stochastic approaches [3] and resilient approaches [4], it is possible to boost the efficiency of the power sector's operations. Intermittency, lower inertia, unpredictable loading patterns, and other challenges are some of the barriers that must be addressed by power systems that are based on renewable energy sources. The interconnection of power networks that run on renewable sources of energy has a number of distinct advantages. However, the transition to renewable energy sources can lead to unstable power systems that are slow to react to disruptions [5]. The weak inertial response is the primary factor contributing to the instability of the power grid, as opposed to normal systems that are based on non-renewable resources. Because of their contact with power interface converters, solar and wind production are unable to maintain a considerable inertial response [6]. This is because their capacity to balance power needs is restricted as a result of this interaction. Low inertial responses lead to highly imbalanced power networks and decreased flexibility in harmonic distortion in power grids based on renewable energy [7]. This occurs because low inertial responses reduce the amount of energy that can be distributed throughout the grid. At this point in time, comprehensive wind farm energy incorporation into the grid is steadily rising owing to the plentiful obtainability of wind and the goal of reducing CO2 emissions [8]. On the other hand, because of the unpredictability of wind power, this might result in an imbalance between supply and demand for load, which, in turn, could cause substantial frequency fluctuation issues [9]. This issue may manifest itself in a substantial manner in the primary case where the capability of LFC is inadequate throughout the nighttime hours [10].

Moreover, electric vehicles (EVs) have seen widespread adoption in recent years due to environmental concerns such as a reduction in the use of fossil fuels, lower charging rates, and greenhouse gas emissions [11]. EVs are employed in a broad range of applications because of the intrinsic properties of the technology known as vehicle-to-grid (V2G). Some examples of these applications include the smoothing-out of renewable resources [12] and supplementary services [13], [14]. Due to the rapid dynamic reaction of batteries in electric vehicles (EVs), the use of frequency regulation services with EVs has garnered a lot of interest recently. This response helps counterbalance the average power imbalance that exists in the system when the LFC capability is insufficient. The dynamic performance of the LFC system is improved because of the instantaneous reaction of EVs. When electric vehicles (EVs) take part in frequency regulation services, the

economy as a whole will reap additional benefits from frequency control marketplaces. As a result, the involvement of electric vehicles (EVs) in frequency management issues will soon be promoted. Nevertheless, owing to the complication of controlling a networked, multiple-region system, green transportation has become an issue that poses a challenge to the present load equilibrium methodologies.

B. LITERATURE REVIEW

Many different types of controllers have been proposed in the literature for use in load frequency control (LFC) [15], [16], [17]. These include integer orders, predictive models, fuzzy logic controllers, neural networks, fractional orders, and complex control systems. Various LFC systems have been described in the literature, involving connections between the tilt, derivative, proportional, integrator, and filtered derivative. In [18], the EV-specific PI regulator was introduced. However, there are stability problems related to this regulator, particularly when communication time delays (CTDs) are considered. Using the differential evolution technique, which was described in [18], the tilt integral filtered derivative (TIDF) regulator for RESs-incorporated power grids was able to be tuned for optimal performance. When analyzing the power networks, [19] merged the settings for the PI controller, the TD controller, and the filter controller. An upgraded version of the genetic algorithm (GA) approach and the particle swarm optimizer (PSO) were used in the hybrid technique that was disclosed in [20] for the purpose of building the controller that is utilized to stabilize the frequency of power networks. For multi-generational networks, [21] suggests using a fractional-order regulator whose parameters have been fine-tuned by the imperialist competitive search (ICA) approach. When multiple-step alterations have been considered in the generation and/or loading, the controller that has been described previously is able to successfully improve the performance of the power approach. Cascading the FOPID and FLC is how frequency control is accomplished in power networks that include two distinct areas [22]. In addition, using the grey wolf optimizer method in designing the LFC for multi-generation power networks [23] has been proposed as a decision. The authors in [24] proposed using FOPID with FO filter, and the sine–cosine algorithm (SCA) approach was applied in order to successfully optimize the controller settings. Moreover, [25] suggests an optimum self-tuning fractional order fuzzy (OSTFOF) regulator for improving the frequency performance of a dual-area hybrid power system with the help of the Pathfinder algorithm (PFA), which has been used to optimize the OSTFOF controller parameters as well as the output membership functions. In [26], an IEEE-standards-compliant single-region pumped storage system is presented, together with a FOPID controller-based control strategy for the regional load frequency of the pumped-storage power plants. The chaos particle swarm optimization (CPSO) approach has been used to fine-tune the controller's settings. Furthermore, to establish which is best

for enhancing the frequency stability in a shipboard microgrid that uses several energy sources, PIDF, FOPIDF, and 2DOF-PIDF were all studied by the two researchers of [27]. This research also took into account the lag time introduced by the sensors' and controller's respective communication lines. A bio-inspired optimization algorithm known as the jellyfish search optimizer (JSO) was used to fine-tune these regulators. In order to create the PI-based load frequency controller settings in the most effective way possible, the authors of the paper [28] made use of a technique known as Harris Hawk's approach. Daraz et al. used FOI-TDN for multi-source power grids while taking into consideration a variety of non-linearities [29]. This was accomplished through the utilization of capacitive energy storage. Alterations are made to the recommended procedure's parameters through the utilization of an algorithmic combination that is a combination of SCA and fitness-reliant methodologies.

The authors of [30] employed controlled EVs equipped with bee colony optimizer-based-TIDF regulators. The method of measuring virtual inertia described in [31] has been developed further with the help of PSO. The problems with automatic generation control (AGC) is linked power grids have inspired the development of an ultra-capacitor energy storage device, as described in [32]. Using the pathfinder optimization approach, an improved architecture for the FOTID controller has also been developed [33]. In their study [34], Amil et al. suggested using finely adjusted MFOPID/FOPID regulators for boosting frequency stability in a hybrid power grid. These controllers made use of the jellyfish optimizer. The researchers of [35] provided a novel technique of employing the imperialist competitor strategy to determine the optimal gains of the suggested regulator for frequency regulation power grids. This method was presented as an alternative. Mohamed et al. [36] provide an improved tilt-filtered derivative regulator built on fractional order. This regulator has been optimized using the artificial hummingbird optimizer approach. It was proposed in [37] that the salp swarm method may be used to modify the gains of PID controllers while taking into account two-area networks. In addition, the butterfly optimization strategy was utilized in the development of the dual-stage controller that was presented in [38]. In the study referred to as [39], it was recommended that AGC loops in Power grids with conventional and non-conventional sources should each have their own distinct cascaded FO-ID along with a filter regulator.

It is now abundantly obvious that the body of scholarly work contains a number of LFC concepts that make use of a variety of optimization strategies. The LFC type that is used in conjunction with the optimizer that is chosen has a significant impact on how well the power grid works in response to transients. In addition, a fuzzy logic interface that is dependent on a fault-tolerant compensation control technique has been provided in [40]. This system was designed to protect against simultaneous additive and multiplicative actuator errors as well as nonlinearity in Markov jump networks. In ref. [41],

an illustration was provided for the neural network-based fault-tolerant compensation control problem for Markovian jump networks. In the study referred to as [42], a gorilla troops optimizer has been used for optimum regulation of the flow of network power. This was done in conjunction with the integration of thyristor-controlled series capacitor (TCSC) units, with the goals of increasing voltage stability, lowering fuel costs, and doing away with emanations from power grids. In the paper [43], the authors use a coyote optimization technique to fine-tune a combination of two PI regulators (PI–PI) and PD-PI to manage the frequency regulation in multi-area power grids. In [44], a multiple-region power grid with generation rate restrictions has been fitted with an innovative type two fuzzy PID regulator (T2-FPID) whose settings have been optimized by the water cycle approach (WCA). To eliminate the drawbacks of AC transmission, an arithmetic optimization approach (AOA) has been examined in [45] for the purpose of tuning a fuzzy PID regulator. Their work has taken into account the impact of the high-voltage direct current link. In the paper referenced as [46], a hybrid optimizer, consisting of gravitational search strategy and firefly approach, has been developed in order to fine-tune the suggested regulator settings. This was done so that it could be used for a two-area hydrothermal power grid. In [47], the gains of a fuzzy PID with the added filter to the derivative action have been optimized using the Bees optimization strategy, and the control methodology has been applied to a multi-region linked power grid.

C. CONTRIBUTIONS

Drawing on the aforementioned studies, this paper presents an original attempt to combine the positive aspects of the TIDF, the PIDD, and the fractional derivative regulators in order to provide an exceptional regulator. This controller is known as TIDF-PID$^\mu$D, and its gains are fine-tuned using the Orca Predation Algorithm (OPA), a recently created bio-inspired metaheuristic optimizer that simulates the hunting behavior of orcas and abstracts it into several mathematical models, including driving, encircling, and attacking prey [48]. Following is a list of the principal contributions that can be drawn from this body of work:

● A new and improved load frequency controller (LFC) has been developed, and its name is the TIDF-PID$^\mu$D controller. This controller is based on integrating the TIDF, the PIDD, and the fractional derivative regulators. The utilization of three very effective regulators contributes to an improvement in the performance of stability, quick transients, and reduction of RESs' alterations and loading fluctuations.

● The lately introduced bio-inspired Orca Predation Algorithm (OPA) is the basis for the optimization process suggested for the TIDF-PID$^\mu$D regulator. The suggested OPA-based optimization approach is able to efficiently handle a wide range of optimization problems because it strikes a good balance between the exploration and exploitation phases. When compared to other optimization methods, OPA

TABLE 1. Parameters for power systems x and y and the T-line.

Model Name	Transfer Function Representation	Parameter Symbol	Parameter Value	Parameter Meaning
Power system x	$\dfrac{K_{psx}}{T_{psx} \cdot s + 1}$	K_{psx}, T_{psx}	68.9655, 11.49 s	The gain and time are constant for the power system x
Power system y	$\dfrac{K_{psy}}{T_{psy} \cdot s + 1}$	K_{psy}, T_{psy}	68.9655, 11.49 s	The gain and time constant for power system y
T- line	$\dfrac{2\pi T_{Line}}{s}$	T_{Line}	0.0433	Synchronizing coefficient

not only achieves better precision but also converges much more quickly.

● Demonstrating the efficacy of the recommended TIDF-PID$^\mu$D regulator by comparing its effectiveness to that of a variety of control techniques disclosed in the research literature (for example, FOI-TDN [29] and PIDD2-PD [49] regulators).

● A decentralized electric vehicle (EV) regulator that makes use of the TIDF-PID$^\mu$D regulator introduced in this work. The LFC operation, as well as the EV control capabilities, may both be achieved with the proposed TIDF-PID$^\mu$D.

The remaining parts of the paper are organized as shown below: In Section II, we present a modeling of the explored hybrid system with EV incorporation. In Section III, we describe the control approach and problem presentation. In Section IV, we present the details of the optimization technique that was used in this work (i.e., OPA). In Section V, we present and discuss the results. Finally, in Section VI, we list the conclusions and suggestions for further research.

II. MODELLING OF THE EXAMINED HYBRID SYSTEM WITH EVS INCORPORATION

For the purpose of verifying the new suggested OPA-based TIDF-PID$^\mu$A controller, we employ the two-area linked power grid case study from [36]. Figure 1 depicts the layout and parts of a power grid with an EV system already in place. There are two sections of the electricity grid, designated x, and y. The local load, PV RES plant, and thermal power generation are all located in area x. Alternatively, in area y, there is a wind RES plant in addition to local loads and hydroelectric power generation. It is presumed that electric vehicles are evenly dispersed throughout all of the interconnected power networks.

A. THE CONVENTIONAL POWER SOURCES' MODELS
1) THE MODEL OF THE THERMAL GENERATION UNIT
The thermal power plant model, which is located in area x, consists of a GDB with 0.5% backlash, a reheater, and a thermal turbine with a GRC of 10% pu/minute (0.0017 pu.MW/s), whose transfer functions can be
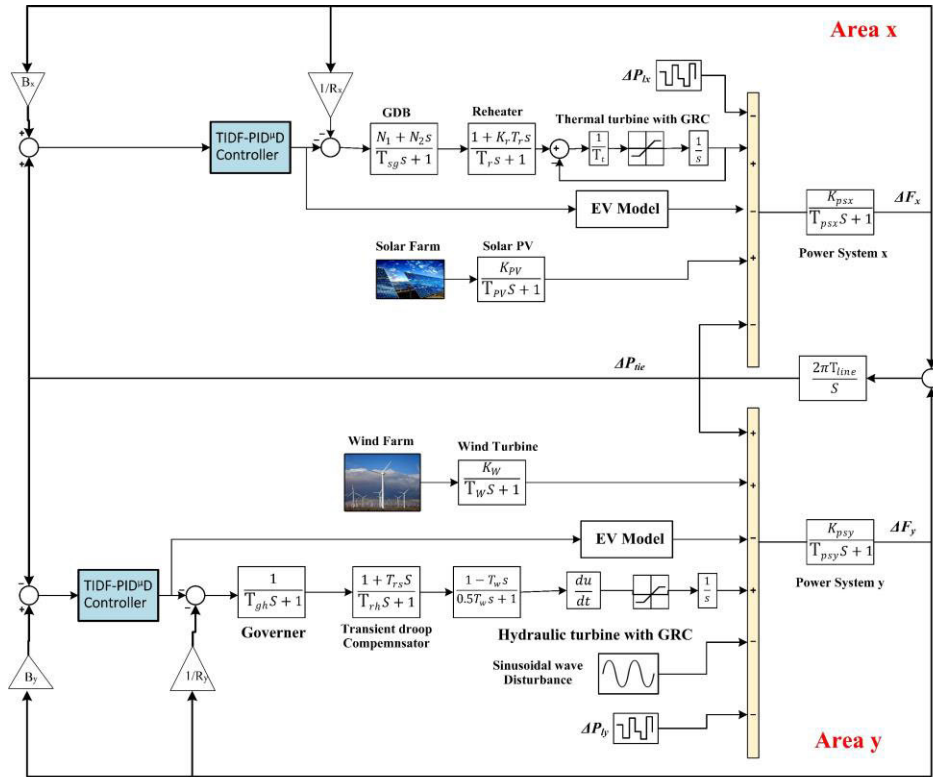
FIGURE 1. The examined power grid in the form of a transfer function model.

formulated as follows [49]:

$$GDB = \frac{N_1 + N_2 \cdot s}{T_{sg} \cdot s + 1} \quad (1)$$

$$Reheater = \frac{k_r T_r \cdot s + 1}{T_r \cdot s + 1} \quad (2)$$

$$Thermal turbine = \frac{1}{T_t \cdot s + 1} \quad (3)$$

where N_1 and N_2 represent the Fourier coefficients whose values are 0.8 and $-0.2/\pi$, respectively; T_{sg} represents the time constant of the steam turbine with a value of 0.06 s; K_r denotes the reheater constant whose value was set as 0.3; T_r depicts the time constant of the reheater whose value is 10.2 s; and T_r denotes the time constant of the thermal turbine and has a value of 0.3 s.

2) THE MODEL OF THE THERMAL GENERATION UNIT
The hydraulic power plant model, which is located in area y, consists of a governor, a transient droop compensator, and a hydraulic turbine with a GRC of 270% pu/minute (0.045 pu.MW/s), whose transfer functions can be formulated as follows [49]:

$$Governor = \frac{1}{T_{gh} \cdot s + 1} \quad (4)$$

$$Transient\ droop\ compensator = \frac{T_{rs} \cdot s + 1}{T_{rh} \cdot s + 1} \quad (5)$$

$$Hydraulic\ turbine = \frac{-T_w \cdot s + 1}{0.5 T_w \cdot s + 1} \quad (6)$$

where T_{gh} represents the time constant of the hydraulic governor with a value of 0.2 s; T_{rs} denotes the hydro turbine speed governor reset time whose value was set as 4.9 s; T_{rh} depicts the time constant of the transient droop compensator whose value is 28.749 s; and T_w denotes the nominal starting time of water in hydro turbine and has a value of 1.1 s.

The thermal and hydro units' governor speed regulation parameters (R_x and R_y) are set at 2.4. The frequency bias coefficients (B_x and B_y) have values of 0.4312. The transfer functions and their parameters' values for Power Systems x and y and the T-line are displayed in Table 1.

B. RENEWABLE ENERGY SOURCES' MODELS
1) THE MODEL OF PV FARM GENERATION
The ambient temperature (T_o) and solar irradiation (θ_s) on the surface of the PV array are the primary factors that influence the power produced by the PV system (P_{out_PV}). The computation P_{out_PV} can be illustrated in the following manner [50]:

$$P_{out\_PV} = P_{STC} \cdot \left(\frac{\theta_s}{\theta_{STC}}\right) \cdot (1 + \alpha(T_o - T_R)) \cdot \eta_M \quad (7)$$

where P_{STC} represents the standard test conditions (STC)-based nominal output power, θ_{STC} stands for the STC-based solar irradiance which has a nominal value
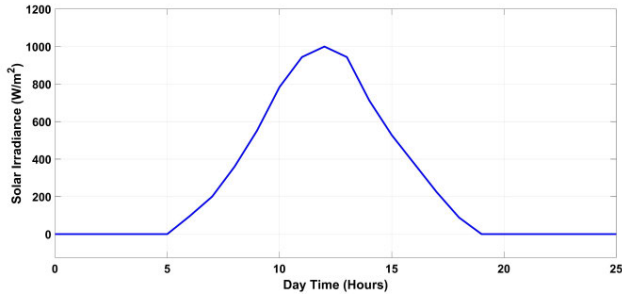
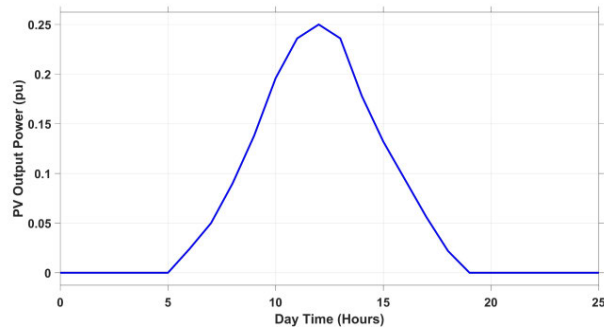**FIGURE 2.** Variation in the amount of solar irradiance [15].

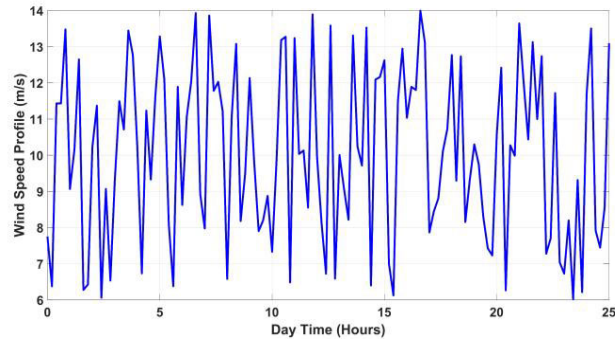**FIGURE 3.** Variability in the power output of PV [15].

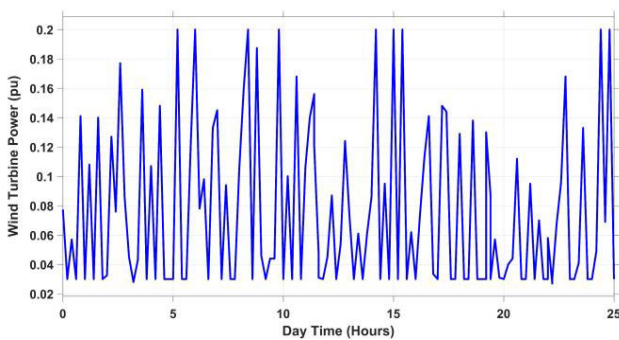**FIGURE 4.** Variability in wind speed observed [15].

FIGURE 5. Variability in the power output of wind turbines [15].
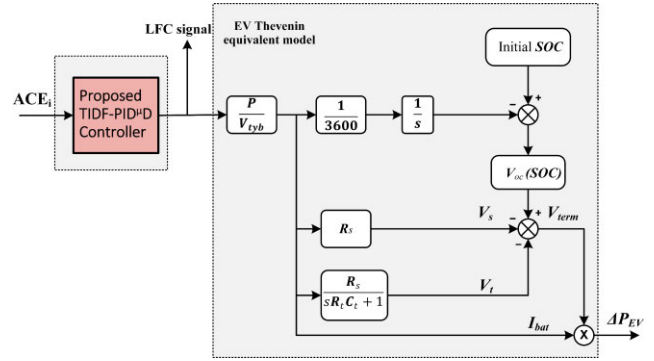

FIGURE 6. The EV model representation corresponds to the Thevenin scheme for load frequency control.

tracking efficiency. Due to the fact that the PV power is linearly proportional to the amount of solar radiation, this research makes use of a straightforward modeling approach for the PV system, which is a transfer function from 1st order described in Equation 8. The PV modeling representation has a gain of one, denoted by the notation K_{PV}, and a time constant of 1.3 s, denoted by the notation T_{PV} [50].

$$PV\ model = \frac{K_{PV}}{T_{PV} \cdot s + 1} \qquad (8)$$

In addition, the input solar radiation that is supplied to the PV modelling representation is gathered from an actual PV station in July 2020 that has a capacity of 1.5 GW and is located in Aswan, Egypt at a latitude of 24.08° North and a longitude of 32.89° East. As can be seen in Figure 2 [15], the solar irradiance at the location follows a normal distribution and reaches a maximum of 1000 W/m^2 at its highest point. In addition, the fluctuation of PV output power, which reaches a maximum of 0.25 pu, is illustrated in Figure 3.

2) THE MODEL OF WIND FARM GENERATION

The ambient equation may be used to determine the power that is produced by a wind turbine generator (P_{out_W}) [50]:

$$P_{out\_W} = 0.5 \cdot C_p \cdot \rho \cdot A_t \cdot V_W^3 \qquad (9)$$

where P_{out_W} represents the output wind power, C_p denotes the power coefficient which is usually controlled to collect the optimal power from the wind unit, ρ stands for the air density in kg/m^3, A_t indicates the swept area of the rotor in m^2, and V_W denotes the wind's nominal speed in m/s.

For the purpose of this investigation, the power-generating system for wind turbines can be represented with a first-order transfer function as in Equation (10). The linear wind turbine model has a gain of one, denoted by K_W, and a time constant of 1.5 s, denoted by T_W [50].

$$Wind\ model = \frac{K_W}{T_W \cdot s + 1} \qquad (10)$$

This analysis also makes use of actual wind speed data from an average wind turbine farm located in the vicinity of Zafarana, Egypt at a latitude of 29.23° North and a longitude
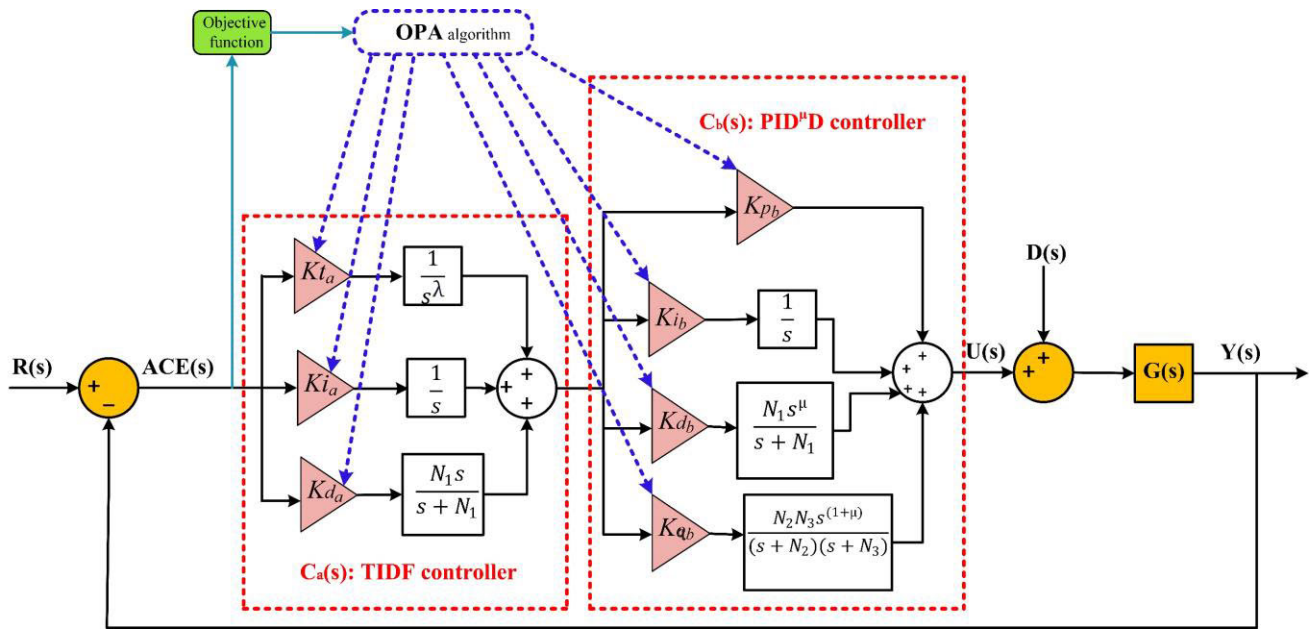
of 1000 W/m^2, α denotes the temperature coefficient, T_R denotes the value of the reference temperature which may be considered as 25°C, and η_M is the maximum power point

FIGURE 7. Structure of the suggested TIDF-PID$^\mu$D controller.

of 32.59° East in April 2020. As may be seen in Figure 4 [15], the average wind speed at this location ranges anywhere from 6 to 14 meters per second. As can be seen in Figure 5, the variance in output power of the wind model varies from a low of 0.03 pu to a high of 0.2 pu throughout the day.

3) THE MODEL OF ELECTRIC VEHICLE (EV)

Recent developments have made it possible for installed EVs to perform the frequency-regulating role. Consequently, the usage of EV batteries allows for better charge/discharge management and less money spent on new energy storage devices. The LFC model requires modeling of the internal battery parameters in order to carry out these supplementary frequency control capabilities. This research assumes that electric vehicles are uniformly dispersed throughout power networks. As may be seen in Figure 6 and as explained in [36], this article implements the usually used Thevenin equivalent model for EVs' design. The open-circuit voltage source (V_{oc}) is a part of the EV Thevenin equivalent model. $V_{oc(SOC)}$ The model represents the source V_{oc}'s dependence on the EV battery's current SOC. The model consists of a shunt RC circuit (R_t, C_t) in addition to a series resistance R_s. The values of R_t, R_s and C_t have been set as 0.047Ω, 0.074Ω and 703.6F, respectively. The RC circuit simulates the consequences of momentary overvoltage. The terminal voltage $V_{term.}$ at an EV's output is calculated by subtracting voltage drops V_s and V_t from $V_{oc(SOC)}$, as shown in Figure 6. Following is the Nernst equation that reflects the relationship between $V_{oc(SOC)}$ and SOC of EV batteries that are currently installed [36]:

$$V_{oc(SOC)} = V_{typ} + S\frac{RT}{F}ln\left(\frac{SOC}{C_{typ} - SOC}\right) \quad (11)$$

where V_{typ} represents the typical voltage, whose value is 364.8 V, C_{typ} denotes the typical capacity of EV batteries which equals 66.2 Ah, S is the sensitivity parameter of $V_{oc(SOC)}$, F stands for Faraday's constant, T indicates the temperature, and R depicts the gas constant. The constant value (i.e., $\frac{RT}{F}$) equals 0.0261. The minimum state-of-charge (SOC) level for the EV's batteries has been set at 10%, while the maximum state-of-charge level (SOC) has been set at 95%. The energy capacity of the EV's battery has been chosen as 24.15 kWh.

III. CONTROL STRATEGY AND PROBLEM PRESENTATION

Despite widespread usage of integer-order PID controllers, more recent studies have shown that conventional regulators lack the efficiency required, particularly for high-order and fractional systems, and this has made the application of fractional regulators in the industry a relatively new area of study. The TID controller is an example of one of these fractional controllers that are utilized for LFC systems. In addition, the filtering phase is included in the derivative part of the TID controller in order to enhance the noise rejection capabilities of the system. The TID with filter, abbreviated as TIDF, has seen widespread use in a variety of power system case studies [51, 21] because it enables simpler adjustment, has a better disturbance rejection ability, and has limited penalties on the plant. So, TIDF was the starting point for the suggested TIDF-PID$^\mu$D controller. As for the second part of the suggested combination, the PIDD controller was selected to play this role, although with certain structural modifications represented by the adoption of fractional derivative action in place of the conventional derivative. The structure of the PIDD controller has been given additional adaptability as a result

of this update. PID$^{\mu}$D is the name that has been given to this newly updated controller. The suggested controller structure accurately depicts the synergistic advantages offered by the various controllers described in the preceding paragraphs.

The TIDF-PID$^{\mu}$D controller has been developed with the goal of enhancing the frequency responsiveness of a power system that integrates both conventional and renewable energy sources in the face of unexpected changes in demand. The controller is recommended in both regions in order to reduce deviations in frequencies and tie-line power (ΔF_x, ΔF_y, and ΔP_{tie}) that occur as a result of various load disturbances and sustainable sources of energy.

A diagrammatic representation of the integrated controller structure may be found in Figure 7. It has the capability to mitigate the negative effect that disturbance D(s) have on the operation of the control system. It was also found that Equation (12) may be used to define the transfer function of the primary loop.

$$Y(s) = (U(s) + D(s)) \cdot G(s) \quad (12)$$

where $G(s)$ stands for the power plant transfer function and $U(s)$ is the suggested controller output signal, which can be considered as the control law input signal to $G(s)$. The control law $U(s)$ may be mathematically represented by Equation (13).

$$U(s) = ACE(s) \cdot C(s) \quad (13)$$

where $ACE(s)$ stands for the area control error signal, and $C(s)$ represents the transfer function of the recommended combination (i.e., TIDF-PID$^{\mu}$D regulator). $C(s)$ may be formulated as follows:

$$C(s) = C_a(s).C_b(s) \quad (14)$$

It is possible to construct the transfer functions of the TIDF and PID$^{\mu}$D regulators by making use of Equations (15), and (16), respectively, in the following manner:

$$C_a(s) = Kt_a\left[\frac{1}{s^{(1/n)}}\right] + Ki_a\left[\frac{1}{s}\right] + Kd_a\left[\frac{N_1 \cdot s}{s + N_1}\right] \quad (15)$$

$$C_b(s) = Kp_b + Ki_b\left[\frac{1}{s}\right] + Kd_b\left[\frac{N_2 \cdot s^{\mu}}{s + N_2}\right]$$
$$+ Ka_b\left[\frac{N_2 \cdot N_3 \cdot s^{(1+\mu)}}{(s + N_2) \cdot (s + N_3)}\right] \quad (16)$$

where the coefficients of TIDF controller (Kt_a, Ki_a, Kd_a, and n) indicate tilt, integral, derivative actions, and tilt FO power, respectively. Whereas the coefficients of PID$^{\mu}$D controller (Kp_b, Ki_b, Kd_b, Ka_b, and μ) indicate proportional, integral, derivative, acceleration actions, and derivative FO operator, respectively. Additionally, the effectiveness of the derivative actions can be improved by N_1, N_2, and N_3, which are the noise filtering parameters.

Reducing the fitness function (FF) will allow the optimal settings for the TIDF-PID$^{\mu}$D controller to be established with the help of the Orca Predation Algorithm (OPA). Because it can shorten the settling time of the output response and

swiftly dampen large oscillations, the integral timed squared error (ITSE) was chosen to serve as the fitness function [50]:

$$FF = \int_0^{t_{sim}} t \cdot \left(\Delta F_x^2 + \Delta F_y^2 + \Delta P_{tie}^2\right) dt \quad (17)$$

where t_{sim} indicates the simulation time, the controller settings are restrained as follows:

$$\begin{cases} Kt_{amin} \leq Kt_a \leq Kt_{amax} \\ Ki_{amin} \leq Ki_a \leq Ki_{amax} \\ Kd_{amin} \leq Kd_a \leq Kd_{amax} \\ n_{min} \leq n \leq n_{max} \\ Kp_{bmin} \leq Kp_b \leq Kp_{bmax} \\ Ki_{bmin} \leq Ki_b \leq Ki_{bmax} \\ Kd_{bmin} \leq Kd_b \leq Kd_{bmax} \\ Ka_{bmin} \leq Ka_b \leq Ka_{bmax} \\ \mu_{min} \leq \mu \leq \mu_{max} \\ N_{1min} \leq N_1 \leq N_{1max} \\ N_{2min} \leq N_2 \leq N_{2max} \\ N_{3min} \leq N_3 \leq N_{3max} \end{cases} \quad (18)$$

where $(f)_{min}$ and $(f)_{max}$ represent the lower and higher bounds of the range of possible values for the tunable controller parameter, respectively. The lower bounds are adjusted to [0, 0, 0, 2, 0, 0, 0, 0, 0, 200, 200, 200] while the higher bounds are chosen as [5, 5, 5, 10, 5, 5, 5, 5, 1, 400, 400, 400].

IV. ORCA PREDATION ALGORITHM (OPA)

In this section, we will provide the bio-inspired optimization technique (i.e., OPA) that was utilized in order to optimize the suggested TIDF-PID$^{\mu}$D controller, as well as provide a mathematical description of the OPA.

A. INITIALIZATION

A pod of orcas composed of N individuals has been established in OPA. The orca is capable of swimming in any dimension, including one, two, three, and even extradimensional space. This leads us to the following formulation of the mathematical model for the orca group:

$$P = \begin{bmatrix} p_1 \ p_2 \ \cdots \ p_N \end{bmatrix} = \begin{bmatrix} p_{1,1} & p_{1,2} & \cdots & p_{1,D} \\ p_{2,1} & p_{2,2} & \cdots & p_{2,D} \\ \vdots & \vdots & \ddots & \vdots \\ p_{N,1} & p_{N,2} & \cdots & p_{N,D} \end{bmatrix} \quad (19)$$

where the symbol P denotes the population size of orcas that resembles the group of all feasible outcomes of the optimization problem. The symbol p_N depicts the location of the Nth orca member, where N represents the number of random values assumed for each parameter of the proposed controller. These parameters include Kt_a, Ki_a, Kd_a, n, Kp_b, Ki_b, Kd_b, Ka_b, μ, N_1, N_2, and N_3. Additionally, $p_{N,D}$ represents the location of Dth dimension of the Nth orca, where D corresponds to the number of controller gains that need to be optimized, which in this case is twelve parameters. Furthermore, Figure 8 presents a lucid representation of the interplay
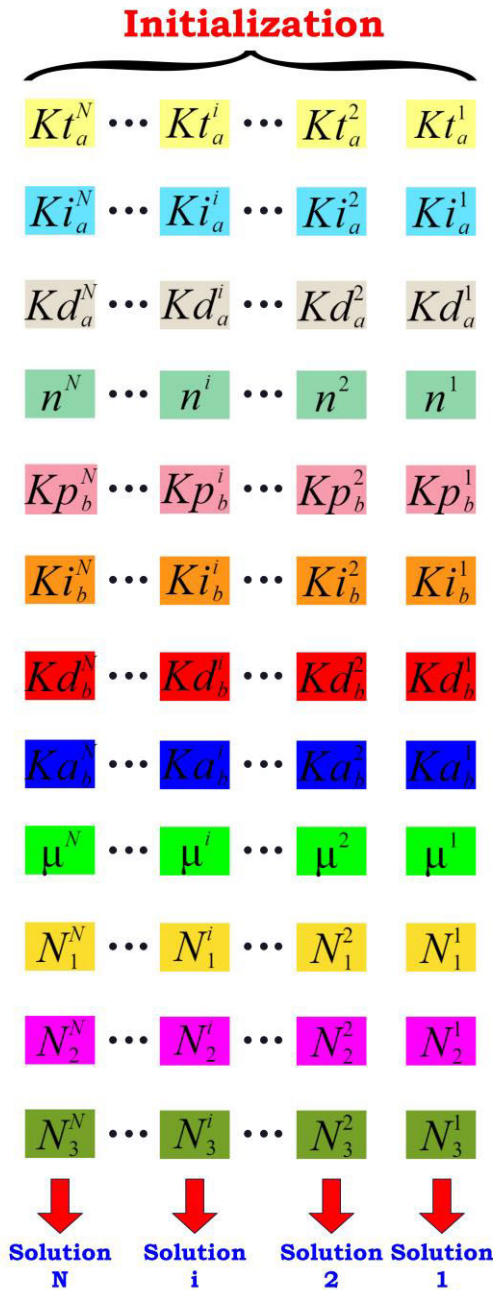
Initialization

$$Kt_a^N \cdots Kt_a^i \cdots Kt_a^2 \quad Kt_a^1$$

$$Ki_a^N \cdots Ki_a^i \cdots Ki_a^2 \quad Ki_a^1$$

$$Kd_a^N \cdots Kd_a^i \cdots Kd_a^2 \quad Kd_a^1$$

$$n^N \cdots n^i \cdots n^2 \quad n^1$$

$$Kp_b^N \cdots Kp_b^i \cdots Kp_b^2 \quad Kp_b^1$$

$$Ki_b^N \cdots Ki_b^i \cdots Ki_b^2 \quad Ki_b^1$$

$$Kd_b^N \cdots Kd_b^i \cdots Kd_b^2 \quad Kd_b^1$$

$$Ka_b^N \cdots Ka_b^i \cdots Ka_b^2 \quad Ka_b^1$$

$$\mu^N \cdots \mu^i \cdots \mu^2 \quad \mu^1$$

$$N_1^N \cdots N_1^i \cdots N_1^2 \quad N_1^1$$

$$N_2^N \cdots N_2^i \cdots N_2^2 \quad N_2^1$$

$$N_3^N \cdots N_3^i \cdots N_3^2 \quad N_3^1$$

| Solution N | Solution i | Solution 2 | Solution 1 |

FIGURE 8. The procedure of initializing the solutions using OPA.

between the OPA and the suggested controller, as well as its use in the adjustment of the prescribed controller settings.

B. CHASING PHASE

Herein, when orcas come upon a group of fish, they don't just circle to pursue; instead, they use sonar to communicate and coordinate their efforts. When the pod of orcas breaks up, they'll scatter, bringing the crowd of fish to the water's surface and herding them into a pen. This observation leads to categorizing the orcas' pursuit stage of hunting into two distinct types: prey driving and prey encircling. A further

parameter, $z1$, is introduced to control the likelihood that the orca will carry out each action independently. It is decided that $z1$ will always be a constant value within the range of $[0, 1]$, and another number between zero and unity will also be created at random. When the number is more than $z1$, the driving stage is executed; otherwise, the encircling stage is accomplished.

1) PREY DRIVING

Once the orcas have identified a shoal of fish, they will need to bring the pod to the surface by pursuing it. Orcas are able to swiftly and correctly determine the location of their prey when the school of orcas that they are hunting in is very small, when the space required to swim is small or the terrain is easy to navigate, hunting is simpler. If a community of orcas is vast, the swimming distance is great, or the scavenging terrain is complex, the orcas' swimming will be easily dispersed, making it impossible to accurately accomplish the goal location. At this time, it is crucial to control the central location of the orca gang so as to keep it nearby the prey while avoiding the orca band from wandering away from its destination, besides permitting individual orcas to approach closer to the prey. This is done so that the pod of orcas doesn't become sidetracked from its mission. The size of the orca population suggests two potential strategies for orca pursuit. The first strategy is utilized if the orca group is big (*rand* is greater than u), while the second strategy is utilized whenever the orca group is tiny (*rand* is less than or equal u).

An illustration of the orca's velocity and its post-movement location is as follows:

$$v_{chase,1,i}^t = g \cdot \left(m \cdot p_{best}^t - F \cdot \left(h \cdot M^t + l \cdot p_i^t \right) \right) \quad (20)$$

$$v_{chase,2,i}^t = e \times p_{best}^t - p_i^t \quad (21)$$

$$M = \frac{\sum_{i=1}^N p_i^t}{N} \quad (22)$$

$$l = 1 - h \quad (23)$$

$$\begin{cases} p_{chase,1,i}^t = p_i^t + v_{chase,1,i}^t & if \ rand > u \\ p_{chase,2,i}^t = p_i^t + v_{chase,2,i}^t & if \ rand \le u \end{cases} \quad (24)$$

where t denotes the cycles' number, $v_{chase,1,i}^t$ is the speed of chasing the ith orca at time t based on the first chasing technique (i.e., Equation (20)), $v_{chase,2,i}^t$ is the speed of chasing of the ith orca at time t based on the second chasing technique (i.e., Equation (21)), M stands for the average location of the orca pod, $p_{chase,1,i}^t$ represents the location of the ith orca at time t based on the first chasing technique, $p_{chase,2,i}^t$ denotes the location of the ith orca at time t based on the second chasing technique, g, h, l and m are arbitrary values between zero and unity, e represents an arbitrary number between zero and two, F is set to 2, and u denotes a number within the range of $[0, 1]$, which describes the possibility of picking a specific chasing technique. The optimal value for u has been adjusted to 0.9 cause the OPA will have the best performance at this value [48].

2) PREY ENCIRCLING

Once the school of fish has been driven to the surface, the orcas must enclose them into a ball under their control. During the encirclement, the orcas use sonar to exchange information and plan their next move based on the whereabouts of the other orcas in the area. In this case, let's suppose that the orcas take their positions according to the locations of three other orcas that were chosen at random. If this is the case, then the position of the orcas, after they move, may be estimated as follows:

$$p_{chase,3,i,k}^t = p_{j1,k}^t + y \times \left(p_{j2,k}^t - p_{j3,k}^t \right) \tag{25}$$

$$y = 2 \times (rand - 0.5) \times \frac{M\_it - t}{M\_it} \tag{26}$$

where M_it stands for the iterations' maximum number, $j1$, $j2$, $j3$ denote the three arbitrarily chosen orcas from N orcas, and $j1 \neq j2 \neq j3$, $p_{chase,3,i,k}^t$ represents the location of the ith orca based on the third chasing technique at time t.

3) POSITIONAL ADJUSTMENTS

Through the use of sonar, orcas are able to determine the location of their prey and modify their own locations appropriately. If the orcas do not sense the advancing of the fish during the operation of pursuing, then they will remain at the initial location. If the orcas see the fish getting closer while they are pursuing it, they will adjust their pursuit to follow the new location. The following equation is used to make the necessary adjustments to their positions:

$$\begin{cases} p_{chase,i}^t = p_{chase,i}^t & if\ fit\left(p_{chase,i}^t\right) < fit\left(p_i^t\right) \\ p_{chase,t}^t = p_i^t & if\ fit\left(p_{chase,i}^t\right) \geq fit\left(p_i^t\right) \end{cases} \tag{27}$$

where $fit\left(p_{chase,i}^t\right)$ is the value of the fitness function related to $p_{chase,i}^t$, and $fit\left(p_i^t\right)$ is the value of the fitness function related to p_i^t. In order to solve the minimal problem, the fitness function index value should be as low as possible. The associated position will be improved as a result.

C. ATTACKING PHASE

Once the orcas have encircled their target, individual orcas will take turns entering the enclosed area to assault the prey, lashing their tails against the circle, and destroying the startled fish. Four orcas are considered to characterize the four best locations for striking in the circle. Other orcas can enter the enclosed space by following the path outlined by the four already inside. After finishing their meal, if the orcas choose to return to the enclosure to be replaced by other orcas, the direction of travel can be modified according to the location of the randomly selected orcas. You may calculate the orca's assault speed and position using the following formulas:

$$v_{attack,1,i}^t = \frac{\left(p_{1st}^t + p_{2nd}^t + p_{3rd}^t + p_{4th}^t\right)}{4} - p_{chase,i}^t \tag{28}$$

$$v_{attack,2,i}^t = \frac{\left(p_{chase,j1}^t + p_{chase,j2}^t + p_{chase,j3}^t\right)}{3} - p_i^t \tag{29}$$

$$p_{attack,i}^t = p_{chase,i}^t + c1 \cdot v_{attack,1,i}^t + c2 \cdot v_{attack,2,i}^t \tag{30}$$

where $v_{attack,1,i}^t$ denotes the ith orca's speed vector to pursuit prey at time t, $v_{attack,2,i}^t$ denotes the ith orca's speed vector to reach the enclosure at time t, p_{1st}^t, p_{2nd}^t, p_{3rd}^t, p_{4th}^t stand for the four orcas in the best location in turn, $j1$, $j2$, $j3$ denote the three arbitrary chosen orcas from N orcas in the chasing phase and $j1 \neq j2 \neq j3$, $p_{attack,i}^t$ depicts the location of the ith orca at time t after the attacking phase, $c1$ represents an arbitrary value between zero and two, and $c2$ represents an arbitrary value within the range of $[-2.5, 2.5]$.

Orcas employ sonar in a manner analogous to the process of pursuit of their prey in order to find it and alter their positions accordingly. When the swarm of fish is under control, one of the orcas will head to the edges of the pod of fish and use its tail to drive the group of fish toward itself so that it may grab some food. Using the following pseudocode, one can determine where the orca's location corresponds to the minimal boundary value (lb) of the possible bounds of the issue. Additionally, the flowchart of the OPA can be seen in Figure 9.

Positional adjustments during the attacking phase

1. If $fit(p_{attack,i}^t) < fit(p_{chase,i}^t)$
2. $\quad p_i^{t+1} = p_{attack,i}^t$
3. Else
4. $\quad u = rand$;
5. $\quad$ For $k = 1 : D$
6. $\quad\quad$ If $u < z2$
7. $\quad\quad\quad p_{j,k}^{t+1} = lb(k)$
8. $\quad\quad$ Else
9. $\quad\quad\quad p_{j,k}^{t+1} = p_{chase,i,k}^t$
10. $\quad\quad$ End
11. $\quad$ End
12. End

V. RESULTS AND DISCUSSION

Considering This research uses a large-scale integration of RESs to test the efficacy of the suggested control method in boosting the frequency stability, taking into consideration various forms of load variation. The goal of this study is to bring the investigated system frequency back to the standard level. The suggested control method is based on the proposed TIDF-PID$^\mu$D regulator, which is optimized using the OPA algorithm to achieve the lowest frequency fluctuations for the investigated power grid. In addition to this, the effectiveness of the recommended control strategy is evaluated and contrasted with the efficacy of other control strategies, namely FOI-TDN and PIDD2-PD. The outcomes of the simulation for the dual-area, multi-unit hybrid power grid that was under investigation were run via MATLAB/SIMULINK®(R2022a) to validate the efficiency of the suggested controller in enhancing the performance of the system that was being analyzed. Calculating the value of the optimal objective function, which is characterized by the ITSE value across iterations, enables one to assess
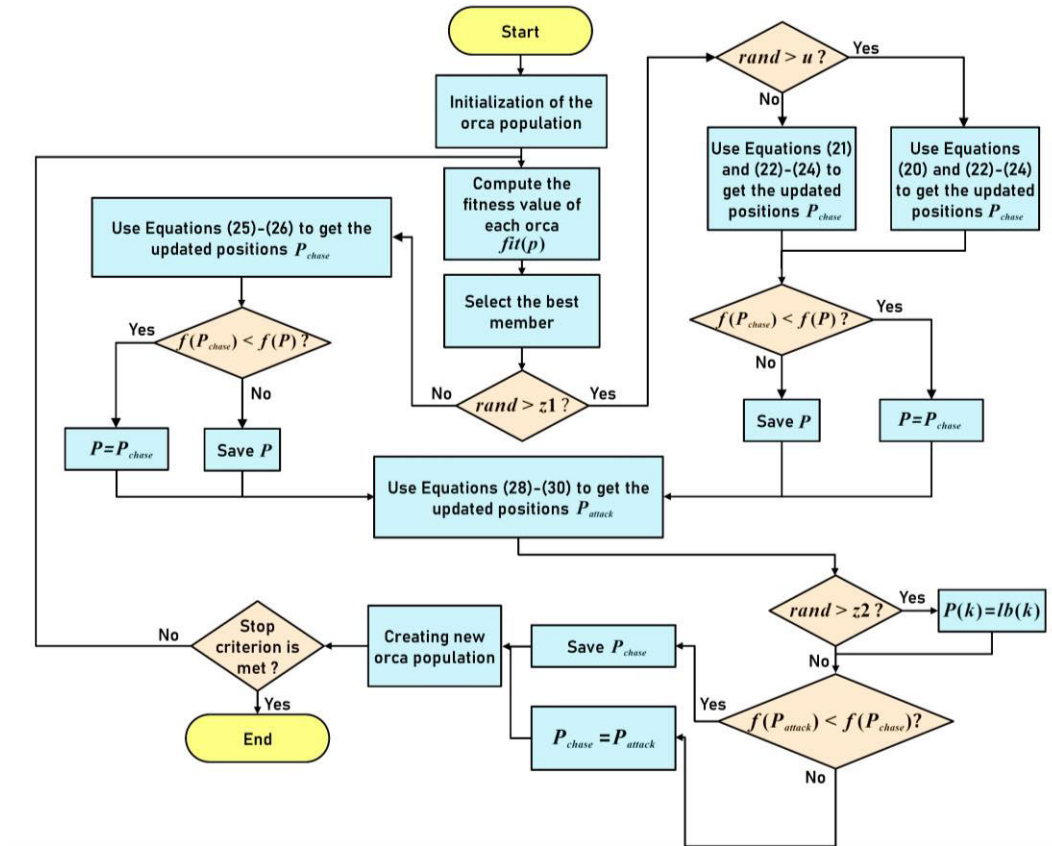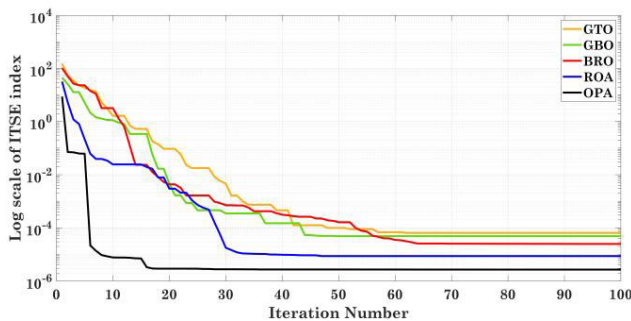
FIGURE 9. The OPA flowchart.

FIGURE 10. The convergence curve characteristics of GTO, GBO, BRO, ROA and OPA.

the efficiency of the power grid that was the subject of the investigation.

Before attempting to optimize the proposed TIDF-PID$^\mu$D regulator using the recommended OPA method, there are a few preliminary concerns that need to be addressed first. These concerns include the 40 populations and the 100 iterations. Figure 10 is a depiction of a convergence curve that highlights the performance of the proposed OPA algorithm in contrast to other contemporary optimization approaches such as the Gorilla Troops Optimizer (GTO), Gradient Based Optimizer (GBO), Battle Royale Optimizer (BRO), and Remora Optimization Algorithm (ROA).When no RES are present in either part of the hybrid power grid under study, the exhibited

convergence curve may be produced by adopting a 1% SLP at 2 sec in area y. When compared to the other alternatives, it is abundantly clear that the OPA algorithm was successful in obtaining the lowest value for the objective function (2.69×10^{-6}). As a consequence of this, the convergence curve provides evidence that the OPA algorithm that has been provided is effective. Furthermore, the performance of the OPA approach is thoroughly evaluated by utilizing seven benchmark functions that have been widely employed in previous research [48]. The efficacy of the OPA is assessed by a comparative analysis with four other metaheuristic algorithms, namely GTO, GBO, BRO, and ROA. For each test function, 30 iterations of each optimization procedure are undertaken. The population size has been fixed at 40 and the maximum number of iterations at 300. The optimal values of the fitness function are presented in Table 2. Figure 11 displays the convergence curves attained by the OPA and other techniques in the benchmark functions that were examined. The findings reinforce the superiority of the OPA in comparison to other approaches.

A. SCENARIO I: 1% STEP DISTURBANCE IMPACT IN AREA Y

So as to confirm the dominance of the presented OPA-based TIDF-PID$^\mu$D regulator over the other recently introduced regulators (i.e., FOI-TDN [26] and PIDD2-PD [49]), which
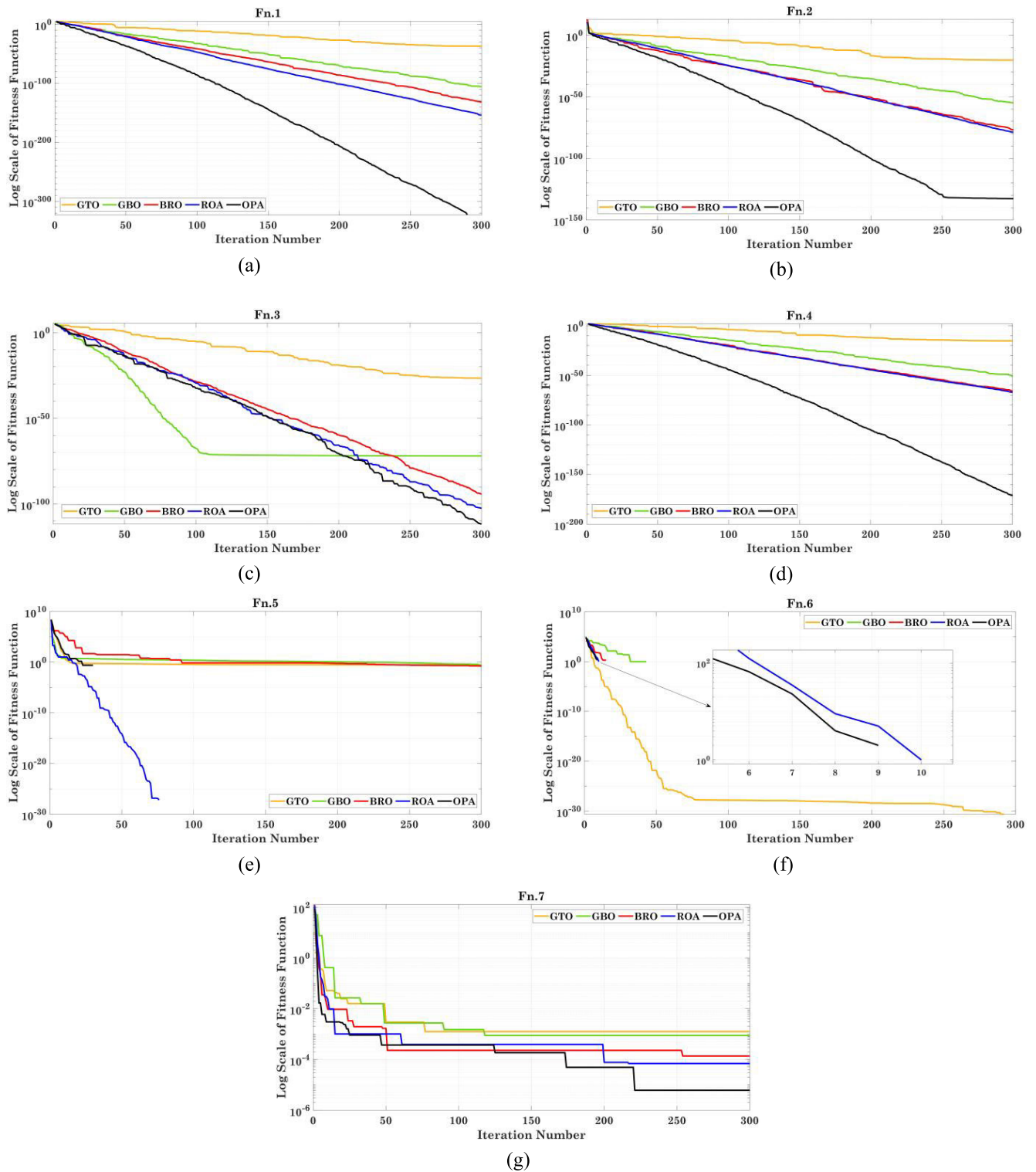
FIGURE 11. The convergence curves of different optimization strategies acquired for several standard benchmark functions.

are also fine-tuned by OPA algorithm, a 1% step load disturbance is applied in area y at t = 2 sec. Table 3 displays the OPA-adjusted regulator gains for this scenario. When creating a comparison with the aforementioned control

approaches, the suggested OPA-based TIDF-PID$^{\mu}$D is outstanding. The frequency and tie-line power responses (ΔF_x, ΔF_y, and ΔP_{tie}) of the examined hybrid power grid system for both area x and area y are depicted in Figure 12,

TABLE 2. The best Fitness functions achieved by the five strategies.

Test Functions		The Best Fitness Function Achieved				
		GTO	GBO	BRO	ROA	OPA
$Fn.\,1(z)$	$\displaystyle\sum_{i=1}^{D} z_i^2$	7.1×10^{-38}	1.7×10^{-106}	1.3×10^{-132}	1.2×10^{-154}	0
$Fn.\,2(z)$	$\displaystyle\sum_{i=1}^{D} |z_i| + \prod_{i=1}^{D} |z_i|$	5.6×10^{-21}	1.3×10^{-55}	1.5×10^{-77}	1.9×10^{-79}	1.8×10^{-133}
$Fn.\,3(z)$	$\displaystyle\sum_{i=1}^{D} \left(\sum_{j=1}^{i} z_j \right)^2$	2.1×10^{-27}	1×10^{-72}	7.4×10^{-95}	3.2×10^{-103}	2×10^{-112}
$Fn.\,4(z)$	$\displaystyle \max_{i}\{|z_i|, 1 \leq i \leq D\}$	5.2×10^{-16}	6×10^{-52}	2.2×10^{-66}	8×10^{-68}	1×10^{-171}
$Fn.\,5(z)$	$\displaystyle\sum_{i=1}^{D-1} \left[100\left(z_{i+1} - z_i^2\right)^2 + (z_i - 1)^2 \right]$	0.2832	0.2223	0.1691	0	0
$Fn.\,6(z)$	$\displaystyle\sum_{i=1}^{D} (|z_i + 0.5|)^2$	0	0	0	0	0
$Fn.\,7(z)$	$\displaystyle\sum_{i=1}^{D} i z_i^4 + rand\,(0,1)$	0.0013	8.8×10^{-4}	1.4×10^{-4}	6.9×10^{-5}	6.1×10^{-6}
Total Computation Time for All Test Functions		1.1873	1.3864	1.3133	1.1821	1.2385

respectively. It has been shown that the recommended OPA-based TIDF-PID$^\mu$D regulator grants improved system stability and improved damping properties with reduced overshoots, undershoots, and settling time than the other regulators. As can be noticed in Figure 12, the presented regulator has attained the lowest ITSE index with a value of 2.69×10^{-6}. Table 4 contains a comprehensive comparative study of the examined controllers for several parameters such as settling time (ST), maximum overshoot (Max.OS), and maximum undershoot (Max.US).

B. SCENARIO II: SEQUENTIAL PULSES IMPACT IN AREA y

Herein, the capability of the suggested OPA-based TIDF-PID$^\mu$D controller is examined under the impact of an increased sequential load pulse profile in area y, where the applied sequential pulse pattern is depicted in Figure 13. Sequential pulses can be considered in real life as a series of connections and disconnection of time-increased load. The system's frequency and power dispersion patterns can be seen in Figure 14 during the impact of the sequential load pulses that the proposed regulator was designed to handle. When compared to the dynamic responses of the other control strategies, the suggested control strategy's dynamic responses have shorter setting times with a small percentage of deviation in their values. The proposed OPA-based TIDF-PID$^\mu$D has effectively maintained the total ITSE index within 0.0376, as shown in the bar graph representation of Figure 15,

TABLE 3. The best settings obtained so far for the controllers under comparison.

| Area	Controller	Controller settings
Area x	FOI-TDN	$K_p = 3.26; K_i = 4.68; K_d = 4.89; \lambda = 0.569; n = 6.12; \mu = 0.891; N = 236;$
	PIDD2-PD	$kp = 32.41; kd = 10.76; nf = 488; KP = 21.63; KI = 47.62; KD = 25.12; KDD = 0.061; ND = 500; NDD = 451;$
	TIDF-PID$^\mu$D	$Kt_a = 1.52; Ki_a = 4.11; Kd_a = 2.49; n = 7.16; Kp_b = 2.02; Ki_b = 5; Kd_b = 4.69; Ka_b = 0.59; \mu = 0.41; N_1 = 400; N_2 = 353; N_3 = 389;$
Area y	FOI-TDN	$K_p = 4.99; K_i = 5; K_d = 4.56; \lambda = 0.82; n = 1.39; \mu = 0.37; N = 500;$
	PIDD2-PD	$kp = 45.36; kd = 34.02; nf = 362; KP = 11.78; KI = 26.17; KD = 11.4; KDD = 0.102; ND = 324; NDD = 269;$
	TIDF-PID$^\mu$D	$Kt_a = 3.44; Ki_a = 4.54; Kd_a = 0.45; n = 3.48; Kp_b = 5; Ki_b = 4.91; Kd_b = 1.83; Ka_b = 0.07; \mu = 0.93; N_1 = 400; N_2 = 278; N_3 = 399;$

which represents the ITSE index for each response (i.e., ΔF_x, ΔF_y, and ΔP_{tie}) as well as the stacked ITSE index for the different controllers. According to Figure 15, the presented
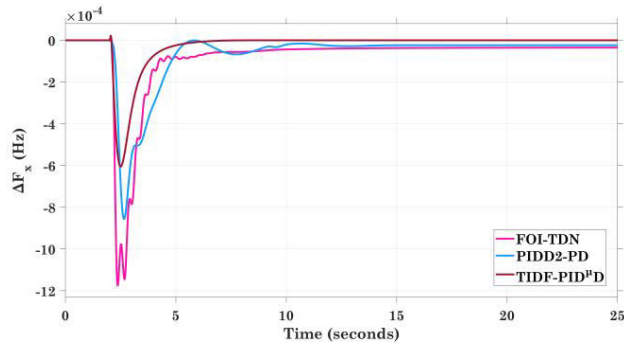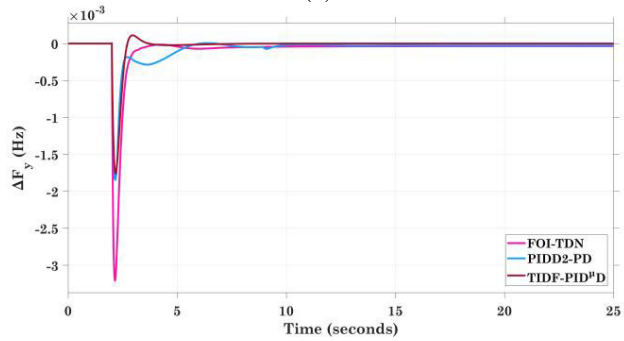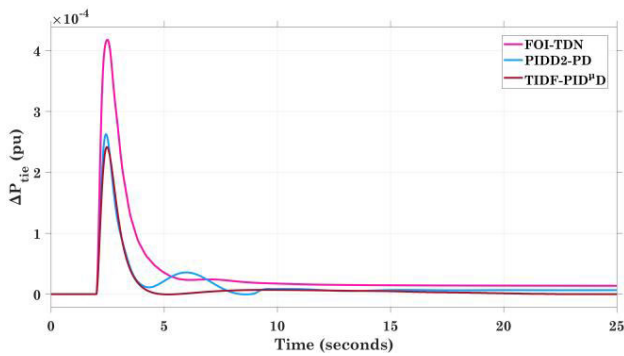
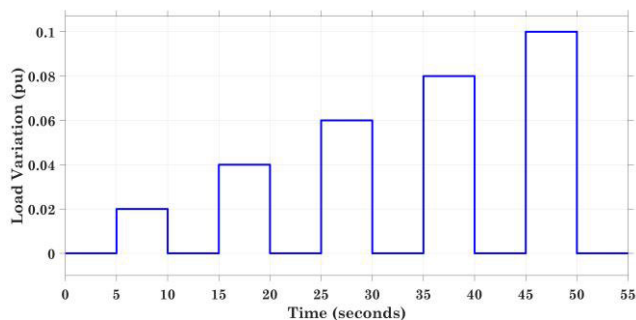**FIGURE 12.** The dynamic characteristics plot representation for Scenario I. (a) ΔFx; (b) ΔFy; (c) ΔPtie.
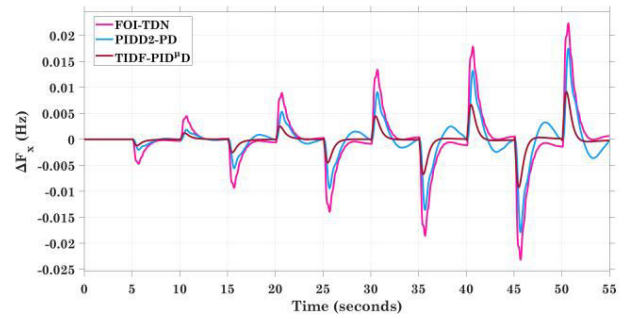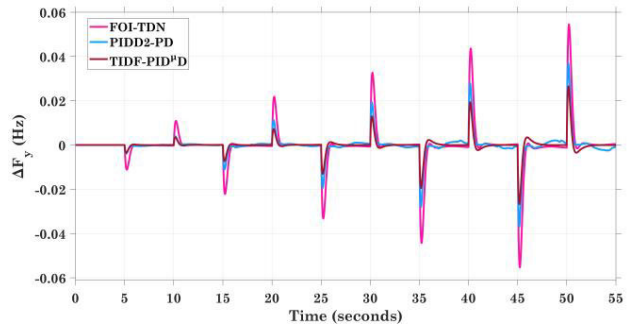

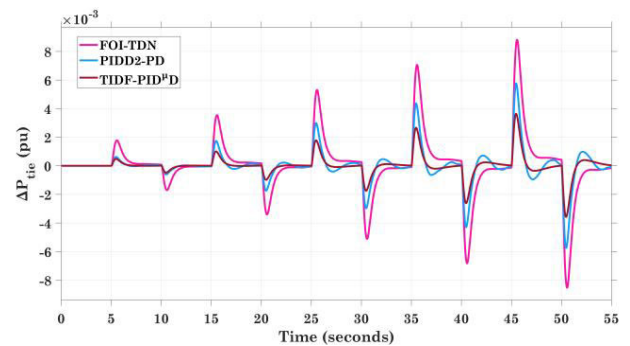**FIGURE 13.** Sequential pulses load variation.

OPA-based TIDF-PID$^\mu$D has achieved an ITSE index that is about 6.39 times less than the FOI-TDN regulator and 2.41 times less than the PIDD2-PD regulator.

FIGURE 14. The dynamic characteristics plot representation for Scenario II. (a) ΔF$_x$; (b) ΔF$_y$; (c) ΔP$_{tie}$.
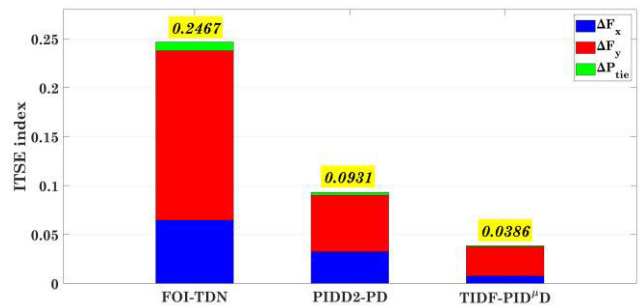

FIGURE 15. The bar graph of the ITSE index for ΔF$_x$, ΔF$_y$, and ΔP$_{tie}$ as well as the Total ITSE index for each controller under the impact of Scenario II.

C. SCENARIO III: SINUSOIDAL DISTURBANCE IMPACT IN AREA y

The analyzed system is put through severe evaluation in this scenario by being exposed to a sinusoidal wave disturbance

TABLE 4. The tabulated dynamic characteristics of the studied hybrid power grid for Scenario I.

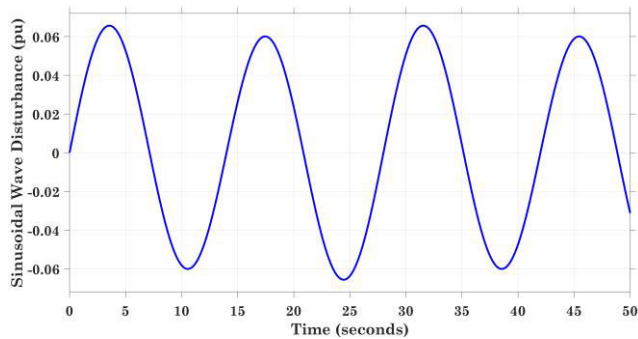| Controller	ΔF_x			ΔF_y			ΔP_{tie}			ITSE
	Max.OS (Hz) $\times 10^{-4}$	Max.US (Hz) $\times 10^{-4}$	ST (s)	Max.OS (Hz) $\times 10^{-3}$	Max.US (Hz) $\times 10^{-3}$	ST (s)	Max.OS (Hz) $\times 10^{-4}$	Max.US (Hz) $\times 10^{-4}$	ST (s)	$\times 10^{-6}$
FOI-TDN	0	-11.89	8	0	3.2	8	4.21	0	7	20.31
PIDD2-PD	0	-8.42	13	0	1.87	5	2.69	0	7	4.53
TIDF-PID$^\mu$D	0	-6	4	0.11	1.75	2	2.46	0	3	2.69

FIGURE 16. Sinusoidal wave disturbance profile.

load profile in region y, which can be shown in Figure 16. In this part, the suggested OPA-based TIDF-PID$^\mu$D has been evaluated, and its efficacy has been examined in relation to the objectives of minimizing frequency and tie-line power variations as well as preserving system stability. This is similar to what was done in the preceding scenarios. Figure 17 illustrates the behavior of the system when subjected to these conditions. The oscillation dampening offered by the combination of TIDF and PID$^\mu$D that has been presented is undeniably superior to that offered by the other combinations that have been evaluated. In addition to this, the OPA-based TIDF-PID$^\mu$D that was developed has successfully kept the overall ITSE index at a value of 0.0039, as can be seen in the bar graph depiction of Figure 18. Figure 18 shows that the suggested controller was successful in acquiring a value of the ITSE that is about 16.13 times lower than the value obtained by the FOI-TDN controller and 2.8 times lower than the value obtained by the PIDD2-PD controller. As a consequence of this, it is abundantly obvious that the combination that was suggested was successful in coping with the various variations and disruptions.

D. SCENARIO IV: WIND AND SOLAR INTEGRATION IMPACT IN BOTH AREAS

This research focuses on high RESs penetration (i.e., the integration of a photovoltaic unit in region x and a wind turbine unit in region y) to evaluate the resilience of the proposed OPA-based TIDF-PID$^\mu$D controller in reducing the investigated system fluctuations. Because of the limitations
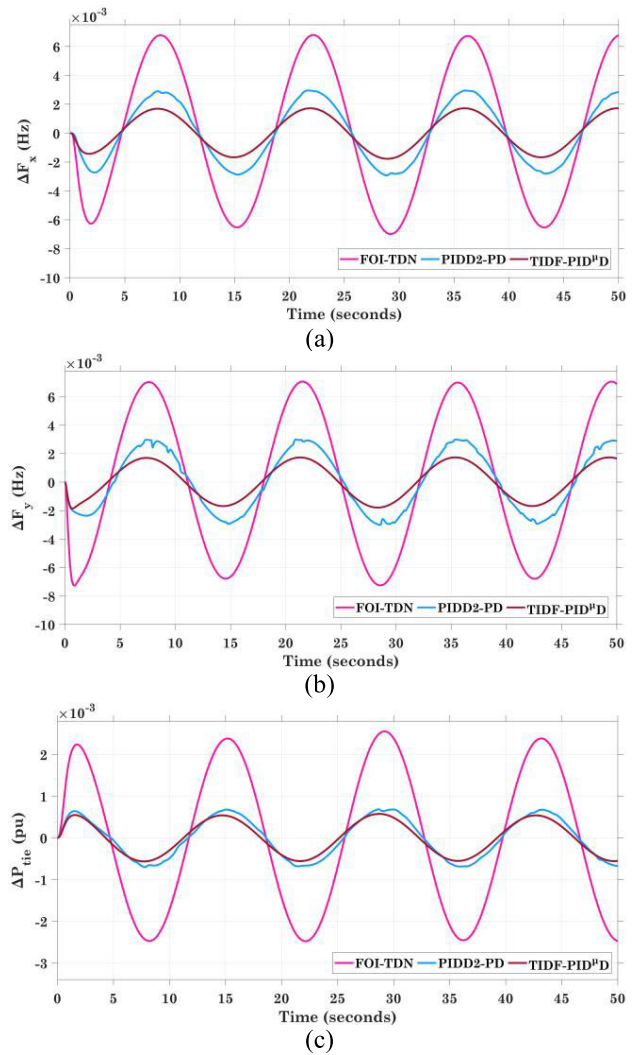

FIGURE 17. The dynamic characteristics plot representation for Scenario III. (a) ΔF_x; (b) ΔF_y; (c) ΔP_{tie}.

associated with these sources (i.e., a lack of inertia in the system), the employment of renewable sources exerts a burden on the hybrid power grid that was explored. The dominance of the recommended TIDF-PID$^\mu$D has been shown and proven through the application of several control architectures, including FOI-TDN and PIDD2-PD regulators based

TABLE 5. The tabulated dynamic characteristics of the studied hybrid power grid for system parameters change.

Controller	Parameter	% Change	ΔF_x			ΔF_y			ΔP_{tie}			ITSE $\times 10^{-6}$
			Max.OS (Hz) $\times 10^{-4}$	Max.US (Hz) $\times 10^{-4}$	ST (s)	Max.OS (Hz) $\times 10^{-3}$	Max.US (Hz) $\times 10^{-3}$	ST (s)	Max.OS (Hz) $\times 10^{-4}$	Max.US (Hz) $\times 10^{-4}$	ST (s)	
TIDF-PID$^\mu$D (proposed)	Normal	0	0	-6	4	0.11	1.75	2	2.46	0	3	2.69
	T_{sg}	+25%	0	-6.78	4.2	0.16	1.79	2.2	2.51	0	3.1	2.75
		−25%	0	-5.63	3.9	0.07	1.72	1.9	2.42	0	2.9	2.63
	T_r	+25%	0	-6.17	4	0.15	1.77	2	2.53	0	3	2.72
		−25%	0	-5.83	4	0.07	1.72	2	2.39	0	3	2.66
	T_{Line}	+25%	0	-6.45	4.1	0.12	1.77	2.1	2.51	0	3.2	2.73
		−25%	0	-5.37	3.9	0.1	1.74	1.9	2.39	0	2.9	2.61
	B_x	+25%	0	-6.04	4	0.12	1.78	2	2.52	0	3	2.7
		−25%	0	-5.98	4	0.09	1.72	2	2.4	0	3	2.68
	R_y	+25%	0	-6.09	4	0.14	1.76	2	2.48	0	3	2.71
		−25%	0	-5.94	4	0.08	1.75	2	2.41	0	3	2.68
	T_{gh}	+25%	0	-6.14	4	0.11	1.76	2	2.51	0	3	2.7
		−25%	0	-5.87	4	0.1	1.74	2	2.38	0	3	2.67
	T_w	+25%	0	-6.24	4	0.12	1.76	2	2.49	0	3	2.72
		−25%	0	-5.79	4	0.09	1.75	2	2.45	0	3	2.68
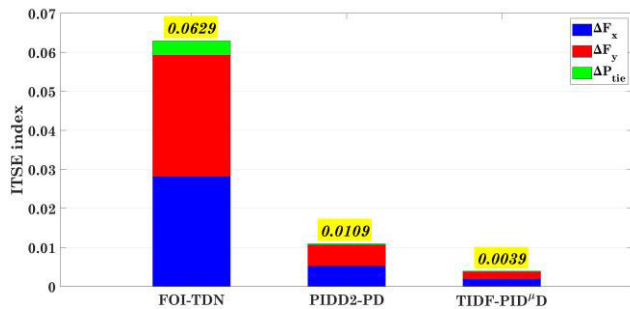
FIGURE 18. The bar graph of the ITSE index for ΔF_x, ΔF_y, and ΔP_{tie} as well as the Total ITSE index for each controller under the impact of Scenario III.

on the OPA. The integration of RESs, as illustrated in Figure 19, generates significant changes in frequency and tie-line power exchange. The system dynamics illustrated in Figure 19 ensure the adaptability and efficacy of the recommended OPA-based TIDF-PID$^\mu$D controller in dampening changes in frequency and tie-line power exchange and improving the performance of the examined power grid. These system dynamics are represented in ΔF_x, ΔF_y, and ΔP_{tie}. The bar graph in Figure 20 depicts the dynamics of the power grid as measured by the ITSE value. The recommended OPA-based TIDF-PID$^\mu$D has the best overall fitness performance for this situation, with an index of 0.0241. This value is about 66.94 times lower than the FOI-TDN controller's claim and 9.65 times lower than the PIDD2-PD controller's claim.

E. CASE V: EVs DISCONNECTION IMPACT

This case describes the incorporation of EVs into both regions of the investigated hybrid interconnected power system in order to evaluate the competence of EVs in managing the investigated system frequency and the flow of power between the two regions. The parameters ΔF_x, ΔF_y, and ΔP_{tie} are used to describe the transient characteristics of the case study in Figure 21. Figure 22 is a bar graph illustrating the dynamic performance of the power system as determined by the ITSE index. If electric vehicles (EVs) are amalgamated into the explored power system, the aggregate ITSE of the system's dynamics decreases to 0.3876, representing an 84.38% improvement. Figure 22 demonstrates that the proposed OPA-based TIDF-PID$^\mu$D that considers the penetration of EVs in the investigated system accomplishes greater system stability than if these vehicles were not taken into consideration. In summary, the investigated integration of electric vehicles (EVs) into the power grid has the potential to reduce frequency fluctuations due to EVs' energy storage capacity. This capacity provides additional power to the system in anomalous situations, ensuring that all of its dynamic responses remain within acceptable limits.

F. SCENARIO VI: SYSTEM PARAMETERS VARIATION IMPACT

This scenario demonstrates the application of sensitivity analysis to assess the robustness of the proposed TIDF-PID$^\mu$D controller by examining the effects of changes in system parameters. In this scenario, several system parameters,
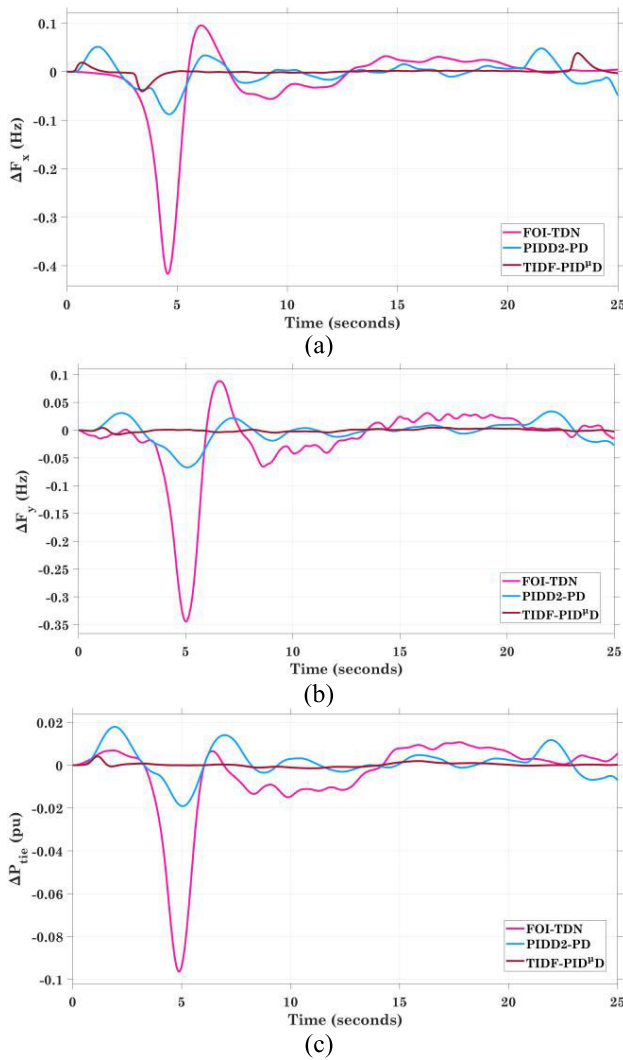
FIGURE 19. The dynamic characteristics plot representation for Scenario IV. (a) ΔF_x; (b) ΔF_y; (c) ΔP_{tie}.
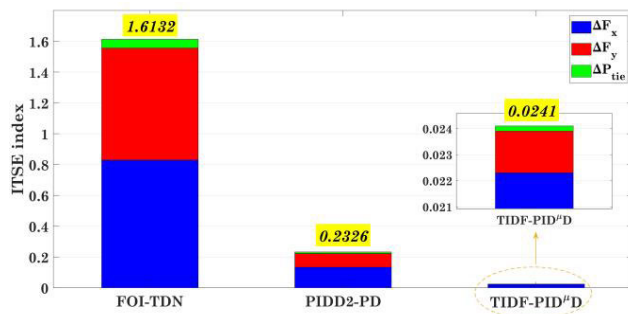
FIGURE 21. The dynamic characteristics plot representation for Scenario V. (a) ΔF_x; (b) ΔF_y; (c) ΔP_{tie}.

FIGURE 20. The bar graph of the ITSE index for ΔF_x, ΔF_y, and ΔP_{tie} as well as the Total ITSE index for each controller under the impact of Scenario IV.
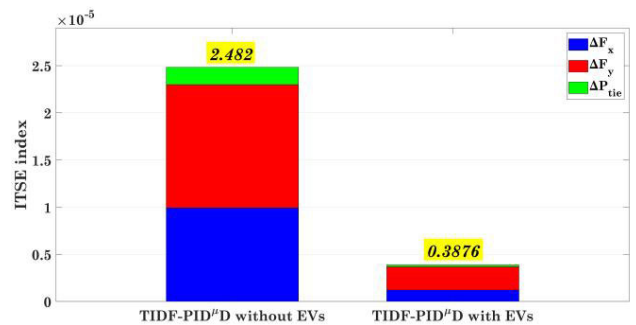
FIGURE 22. The bar graph of the ITSE index for ΔF_x, ΔF_y, and ΔP_{tie} as well as the Total ITSE index for the proposed controller under the impact of Scenario V.

including T_{sg}, T_r, T_{Line}, B_x, R_y, T_{gh}, and T_w, undergo $\pm 25\%$ alteration. The findings of the sensitivity analysis regarding the variation of the aforementioned system parameters are presented in Table 5. It is worth noting that the dynamic responses of ΔF_x, ΔF_y, and ΔP_{tie} exhibit a little impact when

there are changes in these parameters. In addition, the values for Max.OS, Max.US, and ST are still quite low, just like they are when the system is operating normally. Nevertheless, alterations in the remaining system characteristics do not

exert any influence on the dynamic performance of the suggested system. Consequently, the TIDF-PID$^\mu$D controller that has been suggested exhibits robustness and demonstrates a high level of effectiveness in preserving system stability in the face of variations in system parameters.

VI. CONCLUSION

For the purpose of load frequency management, this research proposes an original mixed regulator that is controlled on both an integer and fractional order basis. The two components that make up the proposed hybrid, which is referred to as TIDF-PID$^\mu$D, are the Tilt Integral Derivative with Filter (TIDF) and the Proportional Integral Derivative Fractional Derivative with Filter (PID$^\mu$D), respectively. In the TIDF-PID$^\mu$D regulator that has been proposed, the benefits of the TIDF regulator, the PIDD regulator, and the fractional derivative regulators have been merged. An innovative method that is based on the recently reported Orca Predation Algorithm (OPA) is employed in the research that has been conducted on dual-area power grids. The goal of this method is to improve the proposed TIDF-PID$^\mu$D parameters in the power grids. The TIDF-PID$^\mu$D regulator that has been suggested is a component of a centralized control plan that takes into consideration the function that electric vehicles (EVs) play. The results of a comparison between the performance of the proposed TIDF-PID$^\mu$D regulator and that of the previously published FOI-TD and PIDD2-PD coupled with filters are encouraging. In addition, the outcomes of the OPA optimizer are compared to those of recently published optimization approaches such as the Gorilla Troops Optimizer (GTO), Gradient Based Optimizer (GBO), Battle Royale Optimizer (BRO), and Remora Optimization Algorithm (ROA), and it has been demonstrated that the OPA optimizer achieves superior results compared to the other optimization strategies. This research investigates the problem of frequency stability in a hybrid two-area power system with thermal and hydraulic turbines by taking into consideration nonlinear limits and the presence of renewable energy sources (RES) such as solar farms, wind farms, and electric vehicles (EVs), among other things. The outcomes of this investigation as well as the sensitivity analysis that has been carried out have proven that the proposed control strategy is superior to all other recent strategies in the literature.

CONFLICTS OF INTEREST

The authors declare no conflict of interest.

REFERENCES

[1] M. U. Jan, A. Xin, M. A. Abdelbaky, H. U. Rehman, and S. Iqbal, "Adaptive and fuzzy PI controllers design for frequency regulation of isolated microgrid integrated with electric vehicles," *IEEE Access*, vol. 8, pp. 87621–87632, 2020.

[2] A. Hassan, M. Aly, A. Elmelegi, L. Nasrat, M. Watanabe, and E. A. Mohamed, "Optimal frequency control of multi-area hybrid power system using new cascaded TID-PIλDμN controller incorporating electric vehicles," *Fractal Fractional*, vol. 6, no. 10, p. 548, Sep. 2022.

[3] D. Xiao, H. Chen, C. Wei, and X. Bai, "Statistical measure for risk-seeking stochastic wind power offering strategies in electricity markets," *J. Modern Power Syst. Clean Energy*, vol. 10, no. 5, pp. 1437–1442, Sep. 2022.

[4] M. M. Gulzar, S. Murawwat, D. Sibtain, K. Shahid, I. Javed, and Y. Gui, "Modified cascaded controller design constructed on fractional operator 'β' to mitigate frequency fluctuations for sustainable operation of power systems," *Energies*, vol. 15, no. 20, p. 7814, Oct. 2022.

[5] P. Zhang, A. Daraz, S. A. Malik, C. Sun, A. Basit, and G. Zhang, "Multi-resolution based PID controller for frequency regulation of a hybrid power system with multiple interconnected systems," *Frontiers Energy Res.*, vol. 10, Feb. 2023, Art. no. 1109063.

[6] Y. Arya, "Effect of electric vehicles on load frequency control in interconnected thermal and hydrothermal power systems utilising CF-FOIDF controller," *IET Gener. Transm. Distrib.*, vol. 14, pp. 2666–2675, May 2020.

[7] S. A. Zaid, A. Bakeer, G. Magdy, H. Albalawi, A. M. Kassem, M. E. El-Shimy, H. AbdelMeguid, and B. Manqarah, "A new intelligent fractional-order load frequency control for interconnected modern power systems with virtual inertia control," *Fractal Fractional*, vol. 7, no. 1, p. 62, Jan. 2023.

[8] M. H. Khooban, T. Niknam, F. Blaabjerg, and T. Dragičević, "A new load frequency control strategy for micro-grids with considering electrical vehicles," *Electric Power Syst. Res.*, vol. 143, pp. 585–598, Feb. 2017.

[9] I. D. Margaris, S. A. Papathanassiou, N. D. Hatziargyriou, A. D. Hansen, and P. Sorensen, "Frequency control in autonomous power systems with high wind power penetration," *IEEE Trans. Sustain. Energy*, vol. 3, no. 2, pp. 189–199, Apr. 2012.

[10] S. Kerscher and P. Arboleya, "The key role of aggregators in the energy transition under the latest European regulatory framework," *Int. J. Electr. Power Energy Syst.*, vol. 134, Jan. 2022, Art. no. 107361.

[11] X. Zhu, M. Xia, and H.-D. Chiang, "Coordinated sectional droop charging control for EV aggregator enhancing frequency stability of microgrid with high penetration of renewable energy sources," *Appl. Energy*, vol. 210, pp. 936–943, Jan. 2018.

[12] Y. Zheng, Y. Shang, Z. Shao, and L. Jian, "A novel real-time scheduling strategy with near-linear complexity for integrating large-scale electric vehicles into smart grid," *Appl. Energy*, vol. 217, pp. 1–13, May 2018.

[13] H. Liu, Z. Hu, Y. Song, and J. Lin, "Decentralized vehicle-to-grid control for primary frequency regulation considering charging demands," *IEEE Trans. Power Syst.*, vol. 28, no. 3, pp. 3480–3489, Aug. 2013.

[14] T. Masuta and A. Yokoyama, "Supplementary load frequency control by use of a number of both electric vehicles and heat pump water heaters," *IEEE Trans. Smart Grid*, vol. 3, no. 3, pp. 1253–1262, Sep. 2012.

[15] M. Alharbi, M. Ragab, K. M. AboRas, H. Kotb, M. Dashtdar, M. Shouran, and E. Elgamli, "Innovative AVR-LFC design for a multi-area power system using hybrid fractional-order PI and PIDD2 controllers based on dandelion optimizer," *Mathematics*, vol. 11, no. 6, p. 1387, Mar. 2023.

[16] K. M. AboRas, M. Ragab, M. Shouran, S. Alghamdi, and H. Kotb, "Voltage and frequency regulation in smart grids via a unique fuzzy PIDD2 controller optimized by gradient-based optimization algorithm," *Energy Rep.*, vol. 9, pp. 1201–1235, Dec. 2023.

[17] C.-T. Pan and C.-M. Liaw, "An adaptive controller for power system load-frequency control," *IEEE Trans. Power Syst.*, vol. 4, no. 1, pp. 122–128, Feb. 1989.

[18] Y. Arya and N. Kumar, "BFOA-scaled fractional order fuzzy PID controller applied to AGC of multi-area multi-source electric power generating systems," *Swarm Evol. Comput.*, vol. 32, pp. 202–218, Feb. 2017.

[19] R. K. Sahu, S. Panda, A. Biswal, and G. T. C. Sekhar, "Design and analysis of tilt integral derivative controller with filter for load frequency control of multi-area interconnected power systems," *ISA Trans.*, vol. 61, pp. 251–264, Mar. 2016.

[20] S. Malik and S. Suhag, "A novel SSA tuned PI-TDF control scheme for mitigation of frequency excursions in hybrid power system," *Smart Sci.*, vol. 8, no. 4, pp. 202–218, Oct. 2020.

[21] A. Elmelegi, E. A. Mohamed, M. Aly, E. M. Ahmed, A.-A.-A. Mohamed, and O. Elbaksawi, "Optimized tilt fractional order cooperative controllers for preserving frequency stability in renewable energy-based power systems," *IEEE Access*, vol. 9, pp. 8261–8277, 2021.

[22] Y. Arya, "A new optimized fuzzy FOPI-FOPD controller for automatic generation control of electric power systems," *J. Franklin Inst.*, vol. 356, no. 11, pp. 5611–5629, Jul. 2019.

[23] N. Paliwal, L. Srivastava, and M. Pandit, "Application of grey wolf optimization algorithm for load frequency control in multi-source single area power system," *Evol. Intell.*, vol. 15, no. 1, pp. 563–584, Mar. 2022.

[24] M. S. Ayas and E. Sahin, "FOPID controller with fractional filter for an automatic voltage regulator," *Comput. Electr. Eng.*, vol. 90, Mar. 2021, Art. no. 106895.

[25] A.-A. Zamani, M. Shafiee, and M. Sajadinia, "Optimal self-tuning fractional order fuzzy load frequency control considering sustainable energy sources and electric vehicle," *Int. J. Ambient Energy*, vol. 44, pp. 1–15, Jun. 2023.

[26] X. Gong, K. Yang, X. Dong, X. Jiang, D. Liu, and Z. Luo, "Fractional order PID optimal control method of regional load frequency containing pumped storage plants," *Energies*, vol. 16, no. 4, p. 1703, Feb. 2023.

[27] Y. L. Karnavas and E. Nivolianiti, "Optimal load frequency control of a hybrid electric shipboard microgrid using jellyfish search optimization algorithm," *Appl. Sci.*, vol. 13, no. 10, p. 6128, May 2023.

[28] D. Yousri, T. S. Babu, and A. Fathy, "Recent methodology based Harris hawks optimizer for designing load frequency control incorporated in multi-interconnected renewable energy plants," *Sustain. Energy, Grids Netw.*, vol. 22, Jun. 2020, Art. no. 100352.

[29] A. Daraz, S. A. Malik, A. T. Azar, S. Aslam, T. Alkhalifah, and F. Alturise, "Optimized fractional order integral-tilt derivative controller for frequency regulation of interconnected diverse renewable energy resources," *IEEE Access*, vol. 10, pp. 43514–43527, 2022.

[30] A. Oshnoei, R. Khezri, S. M. Muyeen, S. Oshnoei, and F. Blaabjerg, "Automatic generation control incorporating electric vehicles," *Electric Power Compon. Syst.*, vol. 47, no. 8, pp. 720–732, May 2019.

[31] G. Magdy, A. Bakeer, M. Nour, and E. Petlenkov, "A new virtual synchronous generator design based on the SMES system for frequency stability of low-inertia power grids," *Energies*, vol. 13, no. 21, p. 5641, Oct. 2020.

[32] Y. Arya, "Impact of ultra-capacitor on automatic generation control of electric energy systems using an optimal FFOID controller," *Int. J. Energy Res.*, vol. 43, pp. 8765–8778, Aug. 2019.

[33] S. Priyadarshani, K. R. Subhashini, and J. K. Satapathy, "Pathfinder algorithm optimized fractional order tilt-integral-derivative (FOTID) controller for automatic generation control of multi-source power system," *Microsyst. Technol.*, vol. 27, no. 1, pp. 23–35, Jan. 2021.

[34] A. Daraz, S. A. Malik, A. Basit, S. Aslam, and G. Zhang, "Modified FOPID controller for frequency regulation of a hybrid interconnected system of conventional and renewable energy sources," *Fractal Fractional*, vol. 7, no. 1, p. 89, Jan. 2023.

[35] Y. Arya, "Impact of hydrogen Aqua electrolyzer-fuel cell units on automatic generation control of power systems with a new optimal fuzzy TIDF-II controller," *Renew. Energy*, vol. 139, pp. 468–482, Aug. 2019.

[36] E. A. Mohamed, M. Aly, and M. Watanabe, "New tilt fractional-order integral derivative with fractional filter (TFOIDFF) controller with artificial hummingbird optimizer for LFC in renewable energy power grids," *Mathematics*, vol. 10, no. 16, p. 3006, Aug. 2022.

[37] H. M. Hasanien and A. A. El-Fergany, "Salp swarm algorithm-based optimal load frequency control of hybrid renewable power systems with communication delay and excitation cross-coupling effect," *Electric Power Syst. Res.*, vol. 176, Nov. 2019, Art. no. 105938.

[38] A. Latif, S. M. S. Hussain, D. C. Das, and T. S. Ustun, "Optimum synthesis of a BOA optimized novel dual-stage PI-(1 + ID) controller for frequency response of a microgrid," *Energies*, vol. 13, no. 13, p. 3446, Jul. 2020.

[39] Y. Arya, N. Kumar, P. Dahiya, G. Sharma, E. Çelik, S. Dhundhara, and M. Sharma, "Cascade-I$^{\lambda}$d$^{\mu}$n controller design for AGC of thermal and hydro-thermal power systems integrated with renewable energy sources," *IET Renew. Power Gener.*, vol. 15, no. 3, pp. 504–520, Feb. 2021.

[40] H. Yang, Y. Jiang, and S. Yin, "Adaptive fuzzy fault-tolerant control for Markov jump systems with additive and multiplicative actuator faults," *IEEE Trans. Fuzzy Syst.*, vol. 29, no. 4, pp. 772–785, Apr. 2021.

[41] H. Yang, S. Yin, and O. Kaynak, "Neural network-based adaptive fault-tolerant control for Markovian jump systems with nonlinearity and actuator faults," *IEEE Trans. Syst., Man, Cybern., Syst.*, vol. 51, no. 6, pp. 3687–3698, Jun. 2021.

[42] A. Ginidi, E. Elattar, A. Shaheen, A. Elsayed, R. El-Sehiemy, and H. Dorrah, "Optimal power flow incorporating thyristor-controlled series capacitors using the gorilla troops algorithm," *Int. Trans. Electr. Energy Syst.*, vol. 2022, pp. 1–23, Aug. 2022.

[43] A. A. Abou El-Ela, R. A. El-Sehiemy, A. M. Shaheen, and A. E.-G. Diab, "Enhanced coyote optimizer-based cascaded load frequency controllers in multi-area power systems with renewable," *Neural Comput. Appl.*, vol. 33, no. 14, pp. 8459–8477, Jul. 2021.

[44] C. Kalyan, B. Goud, C. Reddy, H. Ramadan, M. Bajaj, and Z. Ali, "Water cycle algorithm optimized type II fuzzy controller for load frequency control of a multi-area, multi-fuel system with communication time delays," *Energies*, vol. 14, no. 17, p. 5387, Aug. 2021.

[45] A. H. A. Elkasem, M. Khamies, G. Magdy, I. B. M. Taha, and S. Kamel, "Frequency stability of AC/DC interconnected power systems with wind energy using arithmetic optimization algorithm-based fuzzy-PID controller," *Sustainability*, vol. 13, no. 21, p. 12095, Nov. 2021.

[46] D. K. Gupta, A. K. Soni, A. V. Jha, S. K. Mishra, B. Appasani, A. Srinivasulu, N. Bizon, and P. Thounthong, "Hybrid gravitational–firefly algorithm-based load frequency control for hydrothermal two-area system," *Mathematics*, vol. 9, no. 7, p. 712, Mar. 2021.

[47] M. Shouran, F. Anayi, M. Packianather, and M. Habil, "Load frequency control based on the bees algorithm for the great Britain power system," *Designs*, vol. 5, no. 3, p. 50, Aug. 2021.

[48] Y. Jiang, Q. Wu, S. Zhu, and L. Zhang, "Orca predation algorithm: A novel bio-inspired algorithm for global optimization problems," *Exp. Syst. Appl.*, vol. 188, Feb. 2022, Art. no. 116026.

[49] M. Khudhair, M. Ragab, K. M. AboRas, and N. H. Abbasy, "Robust control of frequency variations for a multi-area power system in smart grid using a newly wild horse optimized combination of PIDD2 and PD controllers," *Sustainability*, vol. 14, no. 13, p. 8223, Jul. 2022.

[50] M. Ali, H. Kotb, K. M. Aboras, and N. H. Abbasy, "Design of cascaded PI-fractional order PID controller for improving the frequency response of hybrid microgrid system using gorilla troops optimizer," *IEEE Access*, vol. 9, pp. 150715–150732, 2021.

[51] E. M. Ahmed, E. A. Mohamed, A. Selim, M. Aly, A. Alsadi, W. Alhosaini, H. Alnuman, and H. A. Ramadan, "Improving load frequency control performance in interconnected power systems with a new optimal high degree of freedom cascaded FOTPID-TIDF controller," *Ain Shams Eng. J.*, vol. 14, no. 10, Oct. 2023, Art. no. 102207.

MOHAMMED H. ALQAHTANI (Member, IEEE) was born in October 1989. He received the B.S. degree in electrical engineering from Prince Sattam Bin Abdulaziz University, Saudi Arabia, in 2012, the M.S. degree from the University of South Florida (USF), in 2016, and the Ph.D. degree from the USF Smart Grid Power Systems Laboratory, in 2021. He joined the USF Smart Grid Power Systems Laboratory, in 2017. Currently, he is an Assistant Professor with Prince Sattam Bin Abdulaziz University. His research interest includes power system computing and modeling.

ALI S. ALJUMAH was born in July 1989. He received the B.Sc. degree in electrical engineering from the King Fahd University of Petroleum and Minerals (KFUPM), Saudi Arabia, in 2012, and the M.Sc. degree and the Ph.D. degree in electrical engineering from the University of South Florida (USF), USA, in 2016 and 2022, respectively.

Currently, he is an Assistant Professor with the Electrical Engineering Department, Prince Sattam Bin Abdulaziz University. His research interests include power systems modeling, stability, and renewable energy sources integration to power grid.

SULAIMAN Z. ALMUTAIRI was born in March 1988. He received the B.Sc. degree from Prince Sattam Bin Abdulaziz University, Alkharj, Saudi Arabia, in 2012, and the M.Sc. degree and the Ph.D. degree in electrical engineering from the University of South Florida, Tampa, USA, in 2016 and 2021, respectively. Currently, he is an Assistant Professor with Prince Sattam Bin Abdulaziz University.

SEADA HUSSEN ADEM was born in Wollo, Ethiopia, in 1992. She received the B.Sc. degree in electrical and computer engineering (power stream) from Haramaya University, in 2015, and the M.Sc. degree in power system engineering from Addis Ababa Science and Technology University, in 2020. From 2021, she is a Ph.D. candidate by Electrical Power Enginering at Adama Scince and Technology University. She is working at the Haramaya Institute of Technology, and also she is serving as an editor and/or reviewer on different international journals. She has published 23 research articles in reputed journals and conferences publications.

ADEL OUBELAID was born in Algeria, in 1991. He received the M.Sc. degree from the Institute of Electrical Engineering and Electronics (formerly known as INELEC), Boumerdes, and the Ph.D. degree from Bejaia University. Presently, he holds the position of an Assistant Professor at Bejaia University, where he dedicates his research efforts to a range of topics, including hybrid electric vehicles, power management algorithms, renewable energy systems, drives, motor control, optimization and microgrids.

KAREEM M. ABORAS received the B.Sc., M.Sc., and Ph.D. degrees in electrical engineering from the Faculty of Engineering, Alexandria University, Alexandria, Egypt, in 2010, 2015, and 2019, respectively. His Ph.D. research work is focused on the performance enhancement of renewable energy conversion systems. Currently, he is an Assistant Professor with the Electrical Power and Machines Department, Faculty of Engineering, Alexandria University. His research interests include power electronics, control, drives, power systems, smart grids, microgrids, power quality, optimizations, electric vehicles, machine learning, modeling, fuel cells, HVDC, and renewable energy systems. He is a Reviewer of IEEE TRANSACTIONS ON ENERGY CONVERSION, *Electric Power Systems Research*, *Smart Science*, *Alexandria Engineering Journal*, IET, *Energy Reports*, IEEE ACCESS, *Cybernetics and Systems*, *Protection and Control of Modern Power Systems* (MDPI), *Journal of Advanced Research in Applied Sciences and Engineering Technology*, *Cogent Engineering*, and Hindawi.

• • •